

Prediction-Enhanced Monte Carlo: A Machine Learning View on Control Variate

Fengpei Li^{*†}, Haoxian Chen^{*}, Jiahe Lin^{*}, Arkin Gupta, Xiaowei Tan, Gang Xu, Yuriy Nevmyvaka
Morgan Stanley

Agostino Capponi, Henry Lam
Department of IEOR, Columbia University,

Abstract. Despite being an essential tool across engineering and finance, Monte Carlo simulation can be computationally intensive, especially in large-scale, path-dependent problems that hinder straightforward parallelization. A natural alternative is to replace simulation with machine learning or surrogate prediction, though this introduces challenges in understanding the resulting errors. We introduce a *Prediction-Enhanced Monte Carlo (PEMC) framework* where we leverage machine learning prediction as control variates, thus maintaining unbiased evaluations instead of the direct use of ML predictors. Traditional control variate methods require knowledge of means and focus on per-sample variance reduction. In contrast, PEMC aims at overall cost-aware variance reduction, eliminating the need for mean knowledge. PEMC leverages pre-trained neural architectures to construct effective control variates and replaces computationally expensive sample-path generation with efficient neural network evaluations. This allows PEMC to address scenarios where no good control variates are known. We showcase the efficacy of PEMC through two production-grade exotic option-pricing problems: swaption pricing in HJM model and the variance swap pricing in a stochastic local volatility model.

Key words: Monte Carlo methods, Exotic Options Pricing, Control Variates, Variance Swaps, Swaptions

* equal contribution

† corresponds to: fengpei.li@morganstanley.com

1. Introduction

Monte Carlo (MC) simulation is a foundational tool in computational finance and other domains where closed-form solutions for complex stochastic models are unavailable. Its principal virtues are unbiasedness and the ability to rigorously quantify uncertainty through confidence intervals. By relying on random sampling, MC provides well-understood statistical guarantees and error assessments. However, Monte Carlo methods face significant challenges when applied to complex, nested, or path-dependent settings. As [Glasserman \(2013a\)](#) notes, “The slow convergence of Monte Carlo - its $O(1/\sqrt{n})$ error after n replications - is a persistent obstacle to its wider use.” In other words, while MC excels at delivering unbiased estimates with reliable uncertainty quantification, it often becomes a “slow evaluation”. For example, in the context of derivative pricing, the challenge is further compounded for path-dependent options. [Hull \(2018\)](#) points out that “for path-dependent options, the entire price path must be simulated, significantly increasing computational complexity.” Similarly, [Broadie and Glasserman \(1996\)](#) state that “in many financial simulations, the value at each time step is a function of the previous step, creating a sequential dependency that hinders straightforward parallelization.”

In recent years, machine learning (ML) prediction methods have emerged as a fast alternative for approximating expensive functions, including prices of options and of other financial derivatives ([Ferguson and Liang \(2018\)](#), [Bayer and Stemper \(2019\)](#)). Neural networks and other ML techniques can learn complex mappings quickly, and once trained, can generate predictions at negligible marginal cost - what practitioners often call “fast evaluation” ([Horváth et al. \(2021\)](#)). However, their black-box nature and lack of inherent statistical control make it difficult to dissect error and impossible to ensure unbiasedness [Hutchinson et al. \(1994\)](#). As a result, pure ML approaches often yield biased estimates with no guaranteed measure of error, making them potentially unsuitable for high-stakes applications like risk management where reliable uncertainty quantification is crucial [Buehler et al. \(2019\)](#).

This tension between MC’s reliability and ML’s efficiency motivates the exploration of classical variance reduction techniques, particularly control variates (CV). Control variates provide a systematic approach to improving MC efficiency by exploiting auxiliary functions with known expectations (Glasserman (2013b), Asmussen and Glynn (2007)). When one finds a quantity that is highly correlated with the target while also possessing an analytically known mean, then the variance reduction could be substantial (Boyle et al. (1997)). However, as in many path-dependent exotic derivatives, under many complex models — effective control variates are simply unavailable (see, for instance, Duffie and Glynn (1995)). As noted in Glasserman (2013b), “some exotic payoffs are so irregular that finding an effective control variate becomes a significant challenge in itself.”

Our work seeks to bridge these two approaches, offering a hybrid framework that leverages the best of both worlds. We propose a novel control variate (CV)-based methodology, termed Prediction Enhanced Monte Carlo (PEMC), which extends the classical MC framework by incorporating modern ML techniques while preserving the unbiasedness and rigorous error quantification of MC. In the context of option pricing, unlike traditional ML applications in pricing derivatives, where models are trained to directly predict option prices, we train a certain conditional expectation as CVs, where we break away from two major characteristics of traditional CVs:

- **Known mean requirement:** Unlike traditional CVs that demand the auxiliary function have a known mean (a challenging condition for complex or irregular payoffs), our approach does not rely on this assumption. Instead, PEMC utilizes ML-optimized predictors that are simple to estimate and still provide effective variance reduction.
- **Per-run variance reduction:** While traditional CV techniques are designed to reduce variance on a per-sample basis—pairing each sample with a corresponding control variate—PEMC takes a broader approach. It focuses on achieving variance reduction across the entire simulation scheme, rather than targeting individual sample variance reduction.

Through a careful combination of classical MC principles and ML innovation, our approach eliminates bias from the black-box nature of ML models while also enjoying the unbiasedness and variance reduction provided by the traditional CV methods. By combining these elements, PEMC provides a principled and scalable framework that addresses the shortcomings of both classical CVs and ML-based methods, achieving reliable and interpretable results even in high-dimensional or irregular settings.

1.1. Our Contribution: A Modernized View of Control Variates

We introduce Prediction-Enhanced Monte Carlo (PEMC), a novel framework for evaluating Monte Carlo, which can be viewed as a modernized view of control variates: rather than searching for a single closed-form control variate with a known mean, we train a flexible predictor that acts as a control variate over the entire scheme. Crucially, the construction maintains unbiasedness and allows for valid statistical inference—just as in MC—while leveraging the representational power of ML models to approximate conditional expectations that can be evaluated efficiently. The key innovation of PEMC lies in relaxing the classical requirement that control variates must have a known mean. This is achieved through a two-stage estimation process: the first stage uses a small number of full simulations to estimate the difference between the target and the predictor, while the second stage computes the predictor average using a large number of computationally inexpensive simulations.

This design makes the full simulation cost modest, despite harnessing a large number of cheap samples to drive down variance of the predictor. Consequently, we achieve a form of variance reduction not just on a per-path basis (as the traditional CV), but scheme-wide: the entire simulation procedure, not a given sample design, is optimized to reduce the effective scheme variance vs scheme cost tradeoff, not the per sample variance vs per sample cost tradeoff. This differs from the defining characteristic of traditional CV methods where one control variate is applied per run. Our PEMC approach modernizes this idea, offering a “scheme-wide” variance reduction that can adapt to complex models and broad ranges of parameters.

Compared to purely machine learning-based methods, PEMC transforms the role of ML in Monte Carlo tasks. Rather than relying on ML as a direct surrogate predictor for the quantity of interest—which often introduces biased approximations with unquantifiable errors—PEMC uses ML to construct a robust, unbiased estimator augmented by modernized control variates. This approach enables fast predictions while maintaining Monte Carlo as the de facto standard of evaluation.

1.2. Literature Review

The literature on enhancing MC with ML approximators is extensive, but existing ML-related methods for control variates and variance reduction often impose stringent conditions that limit their practicality. Techniques such as the reproducing Stein kernel approach (Oates et al. (2017), Li and Zhang (2023)), regularized least squares for CV construction (Portier and Segers (2018), South et al. (2022), Leluc et al. (2021)), and adaptive CV schemes (Henderson and Glynn (2002), Henderson and Simon (2004), Kim and Henderson (2007)), as well as \mathcal{L}^2 function approximation frameworks (Maire (2003)), can in theory deliver powerful improvements—including even “supercanonical” convergence rates. But these methods usually require strict assumptions to ensure that the control variate’s mean is known and that it can be easily integrated into the simulation. In many practical settings, these assumptions fail, thus limiting the application scope of these methods. Even though some approaches can theoretically achieve supercanonical convergence rates, their applicability is limited by these constraints.

In contrast, the Prediction-Enhanced Monte Carlo (PEMC) framework overcomes these constraints by reimagining the control variate paradigm to function effectively in scenarios where auxiliary means are unknown. Unlike the aforementioned methods, PEMC aligns more closely with the recently proposed Prediction-Powered Inference (PPI) approach (Angelopoulos et al. (2023)), particularly in its hybrid methodology that integrates valid, unbiased and classical statistical principles with modern machine learning (ML) techniques. This aligns with recent trends in the evaluation of generative models Zrnic and

Candès (2024), such as large language models (LLMs), where fast and interpretable metrics are increasingly critical. In this context, PPI-type of approaches highlight the value of combining human annotations and automatic predictions to yield unbiased estimates of model performance, even in low-label settings. This innovation is particularly valuable in high-dimensional or irregular settings, such as LLM evaluation, where annotated data may be sparse, but unannotated or simulation-based samples are plentiful Boyeau et al. (2024), Eyre and Madras (2024).

Traditional variance reduction and numerical approximation techniques have a long and established history in computational finance and stochastic modeling. One example conceptually related to PEMC is the *Multilevel Monte Carlo (MLMC)* method, as introduced and popularized by Giles (2015). MLMC exploits a hierarchy of discretizations (e.g., finer and coarser time steps in an SDE simulation) to reduce variance at a fraction of the cost of a naive Monte Carlo approach. Its basic premise involves coupling simulations at different resolution levels so that differences between levels have lower variance, ultimately leading to significant computational savings. Despite its solid theoretical foundations, MLMC can be challenging to implement in practice: constructing suitable couplings between the fine and coarse approximations, ensuring stability, and tuning parameters to achieve the promised complexity gains are all nontrivial tasks. However, adopting a coupling perspective provides valuable insights into how PEMC manages the relationship between the target and the predictor.

The advent of machine learning (ML) has spurred a wave of research aiming to accelerate and improve financial computation, including option pricing. Techniques such as neural network surrogates can approximate pricing functions or Greeks, drastically cutting down on runtime (Hutchinson et al. (1994), Buehler et al. (2019)). However, a major drawback is the lack of rigorous error controls and biases introduced during training.

Our paper is also related to the recent stream of literature in causal inference, where methods aim to mitigate challenges such as selection bias and confounding. Doubly robust

estimators serve as a key example (Bang and Robins (2005)). These estimators maintain consistency even if only one of two specified models—either the outcome model or the propensity score model—is correctly specified. Their inherent idea of robustness through additional predictor resonates with the philosophy behind control variates, as well as PEMC, where pairing a complex estimator with a suitably chosen secondary construct can yield improved stability and reduced variance.

The rest of the paper is organized as follows. In Section 2, we provide a comprehensive background on PEMC. In Section 3, we provide a detailed and comprehensive analysis of the PEMC estimator, presenting both theoretical results and practical illustrations. In Section 4, we apply PEMC to real-world exotic option pricing problems of variance swaps pricing under stochastic (local) volatility models and the pricing of swaptions under the Heath-Jarrow-Morton (HJM) framework. We conclude the paper in Section 5 with discussion on broader implications and potential directions for future research.

2. Prediction-Enhanced Monte Carlo: Framework

In this section, we describe how to apply the “Prediction-Enhanced Monte Carlo” Framework for a general simulation evaluation. While this framework has broad applicability, for clarity and concreteness, we will present it in the context of options pricing. This choice of notation and presentation aligns with our subsequent examples and reflects a significant area of application. However, it’s important to note the principles and methodology we discuss here can be readily adapted to a wide range of problems beyond financial derivatives.

To effectively illustrate our proposed framework, facilitate a comprehensive comparison with traditional methods, and enhance the reader’s understanding, we employ Asian option pricing as a running example throughout in this section. Asian options are path-dependent derivatives whose payoffs depend on the average price of the underlying asset over a specified period. As mentioned in Boyle et al. (1997) and Dingec et al. (2015), closed-form solutions for the pricing of arithmetic average Asian options are generally not available, but arithmetic average Asian options serve as an exemplary case where control variate

methods, based on closed-form pricing of the geometric average Asian option under well-known models, can drastically reduce variance and enhance the efficiency of Monte Carlo simulations. However, as we will demonstrate, our new framework achieves the same level of variance reduction without requiring explicit knowledge of the construction of a control variate or its closed-form mean. This significantly expands the applicability and effectiveness of control variate techniques in arbitrarily complex models.

2.1. Problem Setup

The quantity of interest is an evaluation that can be expressed via:

$$\text{Option Price} = \mathbb{E}_{\text{general risk neutral measure}} [f_{\text{payoff}}(\mathbf{Y})]. \quad (1)$$

Here \mathbf{Y} represents a potentially high-dimensional random quantity that encapsulated all the randomness generated under a general, accessible sampling mechanism, denoted here by a *general risk neutral measure* \mathbb{E} . For example, if one is required to generate a discretized sample path of a certain stochastic differential equation (SDE) using some numerical scheme, \mathbf{Y} then represents a complete sample path generated and the measure induced by that discretized SDE would be the *general risk neutral measure*. Typically, the more complex the simulation scheme is, the higher the dimension of \mathbf{Y} will be, as more sophisticated simulation scheme often requires more intermediate steps or additional variables (e.g., an order of $O(T/\Delta t)$, when T is the time horizon and Δt is the discretization time step). Then, f_{payoff} , denoted by the term *payoff function*, represents the proper function (functional) that transform or summarize \mathbf{Y} into a sample for the quantity of interest. The motivation for our framework arises, when the complexity and generality of the payoff function f_{payoff} leads to a highly complicated dependence on the entirety of the random variables \mathbf{Y} . This complication may stem from factors such as path dependency, nested or multilevel simulations, or intricate interactions within the model. Consequently, drawing valid samples from the distribution of $f_{\text{payoff}}(\mathbf{Y})$ becomes both challenging and computationally intensive.

To fully specify the framework, we need to define the several parameters governing both the risk-neutral measure and the payoff function. We formally list the key definitions as:

1. **Model Parameters** θ_{model} : These are the parameters that specify the simulation or the stochastic model of the underlying process Y (e.g., asset value time series). For instance, in a Heston model (Heston 1993), the price process S_t and the instantaneous volatility process v_t are jointly modeled:

$$\begin{aligned} dS_t &= rS_t dt + \sqrt{v_t} S_t dW_t^S \\ dv_t &= \kappa(\eta - v_t) dt + \delta \sqrt{v_t} dW_t^\gamma \end{aligned} \quad (2)$$

The model parameter θ_{model} is thus 5 dimensional $\theta_{\text{model}} := (r, \eta, \delta, \rho, \kappa) \in \mathbb{R}^5$. It specifies the risk neutral drift r , the long-run average variance η , the volatility of volatility δ , the correlation ρ of between W^S and W^γ , and the mean reversion rate κ . In options pricing, these parameters are typically calibrated to fit market data and then used to generate sample paths $Y := \{S_t\}_t$. Thus θ_{model} governs and describes $\mathbb{E}_{\text{risk neutral measure}}$ that generates Y .

2. **Simulation Parameters** $\theta_{\text{simulation}}$: These parameters also specify $\mathbb{E}_{\text{risk neutral measure}}$. The distinction between $\theta_{\text{simulation}}$ and θ_{model} is somewhat artificial, primarily stemming from the convention that not all simulation parameters are not calibrated externally, but rather serve as hyperparameters of the Monte Carlo simulation itself (either customized or directly observed). For example, when one simulates the Heston model above using Euler discretization scheme,¹ we use $\theta_{\text{simulation}}$ to specify the initial stock price S_0 , the initial volatility v_0 , the time horizon T , and discretization time step Δt . The choice of these parameters can impact both the accuracy and efficiency of the simulation. While not typically part of the model calibration process, these parameters also play a crucial role in describing risk-neutral measure.

¹ As mentioned in Dingee et al. (2015), Euler scheme was the primary method for simulation of Heston model until the exact simulation of Broadie and Kaya (2006) is developed. However, due to its significant computational demands, the exact method is less commonly used in practice and simpler, biased simulation method such as Quadratic Exponential (Andersen 2008) or Euler scheme remains prevalent (see, e.g., Lord et al. (2010)).

3. **Payoff Function Parameters** θ_{payoff} : This parameter θ_{payoff} parametrizes the *payoff function* $f_{\theta_{\text{payoff}}}$. In options pricing, this specifies the details of the contract. For example, given the full price path $Y := \{S_t\}_t$, the payoff function for an arithmetic Asian options takes the form

$$P_A(\{S_t\}_t) = \max\left(\frac{1}{n_D} \sum_{i=1}^{n_D} S_{t_i} - K, 0\right)$$

where θ_{payoff} specifies the strike level K , the sampling frequency n_D and the observation dates $\{t_i\}_{i \in [n_D]}$. Notice we have simply omitted the discount factor e^{-rT} .

Under these definitions, we can summarize the standard Monte Carlo approach as follows: one calibrates θ_{model} , specify $\theta_{\text{simulation}}$ and generate n independent paths $\{Y_i\}_{i \in [n]}$ according to $\mathbb{E}_{\text{risk neutral measure}}$ given by θ_{model} and $\theta_{\text{simulation}}$. Finally, one averages $\frac{1}{n} \sum_i f_{\theta_{\text{payoff}}}(Y_i)$.

Remark Having specified the distinct roles of θ_{model} , $\theta_{\text{simulation}}$ and θ_{payoff} , we will henceforth refer to them collectively as θ when no ambiguity arises.

2.2. Prediction-Enhanced Monte Carlo: Motivation

As we have seen, Asian options are path-dependent derivative securities whose payoffs depend on the average prices of the underlying asset. Closed-form solutions for their prices are generally unavailable, numerous studies have proposed new numerical methods for pricing them (see [Dingec et al. \(2015\)](#)). While Partial Differential Equation (PDE)-based methods and Monte Carlo simulation are both generic methods for pricing options, applying PDE methods to particular models often requires special effort, primarily due to the curse of dimensionality. Moreover, for our discussion here, it has been noted that no PDE method performs well for Asian options under the Heston model [Dingec et al. \(2015\)](#). Therefore, across various models, simulation becomes the common choice. The principal drawback of simulation, as strongly highlighted in the literature, is its slow convergence rate. Employing variance reduction methods is therefore essential to improve the precision of simulation results. However, designing a successful variance reduction method requires exploiting the special structures of the derivative security and the underlying model. As a result,

control variate (CV) techniques are often not available for pricing options under most of the complicated models used in practice. In fact, the pricing of arithmetic Asian option under Black–Scholes geometric Brownian motion (GBM) model is a main exception where the closed-form expression of the geometric Asian option allows one to effectively deploy control variate techniques. However, as soon as one extends beyond the most basic GBM model to more complex models such as the Heston model, the closed-form solutions for the geometric Asian options are no longer available and the applicability of control variate in these contexts is severely limited (see [Dingec et al. \(2015\)](#)).

More generally in the context of options pricing, while widely used, Monte Carlo methods face challenges when applied to complex, path-dependent derivatives. In such simulations, the state at each time step is determined by the state at the previous step, creating a sequential dependency that precludes straightforward parallelization or speedup. Moreover, for the complex *risk neutral measures* or the irregular *payoff functions* encountered in many exotic options pricing problems, effective control variate or variance reduction techniques are frequently unavailable. As a result, the slow convergence of Monte Carlo - its $O(1/\sqrt{n})$ error after n replications - becomes an acute bottleneck and achieving high accuracy often implies a undesirable large number of replications in practice.

To address these challenges, the Prediction-Enhanced Monte Carlo (PEMC) framework is designed to provide a robust and easily accessible mechanism for designing control variates. This novel approach aims to reduce the number of required Monte Carlo samples by generating a machine learning-based control variate that is both highly parallelizable and efficiently evaluable. Crucially, our framework preserves the unbiased nature of the Monte Carlo estimator, a property that [Glasserman \(2013b\)](#) highlights as “fundamental to the wide applicability of Monte Carlo methods in finance,” achieving a remarkable elimination of any potential bias introduced by any black-box prediction model.

2.3. Prediction-Enhanced Monte Carlo: Prediction Model

In this section, we present our PEMC framework, which is centered around an efficient prediction model. In PEMC, we do not specify the training algorithm or model architecture

for this prediction model, as our framework is essentially compatible with any black-box model. However, as we will demonstrate, the squared error loss—a function that is both convex and differentiable—combined with the need for a flexible model family capable of expressing complex dependencies and being straightforward to train using off-the-shelf, easily accessible solvers, makes neural networks an ideal choice.

When applying the PEMC framework, an efficient prediction model refers to one that can process highly parallelizable and computationally efficient input \mathbf{X} , which serves as a strong predictor or good feature [Hastie et al. \(2009\)](#) for predicting $f_{\theta_{\text{payoff}}}(\mathbf{Y})$. In particular, given the whole path \mathbf{Y} , we want to find some input feature $\mathbf{X} := \phi(\mathbf{Y})$ that is some typically low-dimensional transformation ϕ of \mathbf{Y} with:

- Property 1: \mathbf{X} can be regarded as a reasonable predictor for $f_{\theta_{\text{payoff}}}(\mathbf{Y})$. For example, if \mathbf{X} exhibits a significant correlation with $f_{\theta_{\text{payoff}}}(\mathbf{Y})$, it may serve as the basis for a reasonable linear regressor, although our framework far exceeds linear predictors.
- Property 2: While the joint distribution of d is hard to obtain, the marginal distribution of \mathbf{X} allows for efficient and parallelizable simulation.

The selection of an appropriate \mathbf{X} is a pivotal component of our framework, analogous to feature selection in machine learning tasks. This process necessitates domain expertise and a thoughtful evaluation of the specific financial instrument and underlying model. The challenge lies in striking a balance between the predictive capability of \mathbf{X} for $f_{\theta_{\text{payoff}}}(\mathbf{Y})$ and its computational efficiency. In subsequent sections, we will explore the intricacies of this selection process in greater detail, examining its impact on the performance of the PEMC framework through illustrative examples. For now, we proceed under the assumption that a suitable \mathbf{X} has been identified.

We now focus on the pre-training phase of our prediction model. Unlike many machine learning or deep learning tasks, where the quantity and quality of data are critical challenges—and often a core difficulty due to the expense or scarcity of labeled data—in the Monte Carlo setting, we benefit from an effectively unlimited supply of clean, labeled data

that can be generated as needed. The data generation and model training process can be outlined through the following key steps:

1. We first define a parameter space Θ that encompasses all combinations of $\theta := (\theta_{\text{model}}, \theta_{\text{simulation}}, \theta_{\text{payoff}})$ that are of practical interest. This space should cover the range of parameters that would likely be encountered in real-world pricing scenarios on a daily, weekly or monthly basis, depending on the model update frequency.
2. We then draw samples of θ_i from Θ , using uniform sampling or any measure that ensures comprehensive coverage. For each sampled parameter set, we generate one pair ² of $Y(\theta_i)$ and its corresponding $X(\theta_i) := \phi(Y(\theta_i))$. It's important to note that X and Y are coupled in this generation process.
3. For each generated pair, we compute the payoff $f_{\theta_i, \text{payoff}}(Y(\theta_i))$, which serves as a *label* in our training data. The corresponding *feature* vector is comprised of $(\theta_{i, \text{model}}, \theta_{i, \text{simulation}}, \theta_{i, \text{payoff}}, X(\theta_i))$.
4. This process is repeated N_{train} times to generate training dataset which consists of N_{train} pairs of

$$\text{label}_i := (\theta_{i, \text{model}}, \theta_{i, \text{simulation}}, \theta_{i, \text{payoff}}, X(\theta_i))$$

$$\text{feature}_i := f_{\theta_i, \text{payoff}}(Y(\theta_i))$$

for $i \in [N_{\text{train}}]$.

5. The machine learning model g is then trained to minimize the mean squared error (MSE) loss and save the resulting model g :

$$\min_g \frac{1}{N_{\text{train}}} \sum_{i \in [N_{\text{train}}]} (\text{label}_i - g(\text{feature}_i))^2. \quad (3)$$

The essential steps are summarized in Algorithm 1. While the data generation process can be time-intensive due to the complexity of Y , it is conducted offline during the pre-training phase. This approach minimizes its impact on real-time pricing applications by effectively trading memory usage for computational speed during execution.

² You could also generate multiple pair of $(Y(\theta_i), X(\theta_i))$ under the same sampled θ_i .

Algorithm 1 Prediction Model Training

```

1: procedure DATAGENERATION( $N_{\text{train}}, \Theta$ )
2:   Initialize empty datasets (features, labels)
3:   for  $i = 1$  to  $N_{\text{train}}$  do
4:     Sample parameters  $\theta_i \sim \Theta$  uniformly
5:     Generate  $X(\theta_i), Y(\theta_i) \sim \mathbb{E}_{\text{risk neutral measure}(\theta_i)}$ 
6:      $\text{label}_i \leftarrow f_{\theta_i, \text{payoff}}(Y(\theta_i))$ 
7:      $\text{feature}_i \leftarrow (\theta_{i, \text{model}}, \theta_{i, \text{simulation}}, \theta_{i, \text{payoff}}, X(\theta_i))$ 
8:     Store ( $\text{feature}_i, \text{label}_i$ ) to (features, labels)
9:   end for
10:  return datasets (features, labels)
11: end procedure

12: procedure TRAINING(features, labels)
13:  Initialize model  $g$ 
14:   $N_{\text{train}} \leftarrow \text{length}(\text{features})$ 
15:  Minimize:  $\min_g \frac{1}{N_{\text{train}}} \sum_{i \in [N_{\text{train}}]} (\text{label}_i - g(\text{feature}_i))^2$ 
16:  return trained model  $g$ 
17: end procedure

```

This pre-training setup presents an ideal scenario for machine learning applications. Unlike many real-world problems where data scarcity is a concern, access to the data-generating process in PEMC allows for the creation of virtually unlimited, clean data. This abundance greatly facilitates the training of complex models. It is important to also note that PEMC does not require g to take specific forms. However, the convex and differentiable nature of the loss function (i.e., squared loss), the large supply of data (i.e., from Monte Carlo simulation), and the need for expressiveness of the model family make neural networks (NNs) an ideal choice.

When training NNs, various optimization techniques and architectural enhancements—such as the Adam optimizer Kingma and Ba (2014), batch normalization Ioffe and Szegedy (2015), and skip connections He et al. (2016)—can be employed to improve performance. In fact, recent advancements in machine learning technologies have made the training process remarkably accessible and efficient. The availability of open-source, user-friendly frameworks like PyTorch Paszke et al. (2019), TensorFlow Abadi et al. (2016), and JAX Bradbury et al. (2018)—coupled with GPU acceleration and highly optimized C++ backends—has dramatically simplified the process of training models on large datasets. These frameworks support recent neural network architectures, such as Convolutional Neural Networks (CNNs) LeCun et al. (1998), Residual Networks (ResNets) He et al. (2016), and Transformers Vaswani et al. (2017), as well as various Stochastic Gradient Descent (SGD) optimization algorithms Bottou (2010). In applications, we only utilized well-established and widely recognized neural network structures that are now considered common. These models can typically be implemented using just a few lines of code, as they have been incorporated into existing packages and extensively optimized.

Finally, regarding the choice loss function, we note that the goal of the prediction model g is to produce an approximation of the underlying regression function:

$$g(\boldsymbol{\theta}_{\text{model}}, \boldsymbol{\theta}_{\text{simulation}}, \boldsymbol{\theta}_{\text{payoff}}, \mathbf{X}(\boldsymbol{\theta})) \approx \mathbb{E}_{\text{risk neutral measure}(\boldsymbol{\theta})} \left[f_{\boldsymbol{\theta}_{\text{payoff}}}(\mathbf{Y}(\boldsymbol{\theta})) \middle| (\boldsymbol{\theta}_{\text{model}}, \boldsymbol{\theta}_{\text{simulation}}, \boldsymbol{\theta}_{\text{payoff}}, \mathbf{X}(\boldsymbol{\theta})) \right]$$

As we will see, the quality of this approximation will impact the effectiveness of variance reduction, which we shall explore in detail in subsequent sections.

2.4. Prediction-Enhanced Monte Carlo: Evaluation

Having completed the training phase of PEMC, we now turn our attention to the evaluation procedure. This stage employs the pre-trained model to enhance the efficiency of Monte Carlo simulations, and we will demonstrate how control variates are cleverly constructed to achieve variance reduction. The evaluation process proceeds as follows:

1. A specific parameter set $\theta := (\theta_{\text{model}}, \theta_{\text{simulation}}, \theta_{\text{payoff}}) \in \Theta$ is given, e.g., calibrated from market data in real-time, and needs to be used for pricing. These parameters can be determined through combination of calibration, customization, client agreement or external observation.
2. Generate n pairs of $(Y_i, X_i)_{i \in [n]}$, from $\mathbb{E}_{\text{risk neutral measure}(\theta)}$. Here we have suppressed Y 's dependency on θ , as in the evaluation stage only a fixed θ is considered.
3. Based on the marginal distribution of X , independently generate N additional samples of $(\tilde{X}_j)_{j \in [N]}$ from $\mathbb{E}_{\text{risk neutral measure}(\theta)}$, directly according to its marginal distribution. Importantly, these samples are independent of the previous data $(Y_i, X_i)_{i \in [n]}$.
4. Utilize the pre-trained model g to evaluate the PEMC estimator:

$$PEMC := \frac{1}{n} \sum_{i=1}^n (f(Y_i) - g(X_i)) + \frac{1}{N} \sum_{j=1}^N g(\tilde{X}_j) \quad (4)$$

For notational simplicity, we have written $g(X)$ instead of $g(\theta_{\text{model}}, \theta_{\text{simulation}}, \theta_{\text{payoff}}, X)$, and $f(Y)$ instead of $f_{\theta_{\text{payoff}}}(Y)$. A key aspect of this procedure is the relationship between N and n . Typically, we choose N to be one, or several orders of magnitude larger than n . The optimal choice of N versus n , will be discussed Section 3. The PEMC evaluation step is summarized in Algorithm 2.

Algorithm 2 Evaluation

- 1: **procedure** EVALUATION(θ, n, N, g)
 - 2: Generate i.i.d. $(Y_i, X_i)_{i \in [n]}$ from $\mathbb{E}_{\text{risk neutral measure}(\theta)}$
 - 3: Generate i.i.d. $(\tilde{X}_j)_{j \in [N]}$ independently from its marginal in $\mathbb{E}_{\text{risk neutral measure}(\theta)}$
 - 4: Compute $PEMC := \frac{1}{n} \sum_{i=1}^n (f(Y_i) - g(X_i)) + \frac{1}{N} \sum_{j=1}^N g(\tilde{X}_j)$
 - 5: **return** $PEMC$
 - 6: **end procedure**
-

2.5. PEMC: An Example on Asian Options

To demonstrate the PEMC framework, we return to our ongoing example on arithmetic Asian call option under the Heston model. It is worth noting that while the geometric Asian option is a natural control variate in this context, its closed-form expression is not available under the Heston model. To use control variates here, one must resort to sophisticated methods, e.g, numerically approximating the characteristic function [Fusai and Meucci \(2008\)](#) or employing new framework for conditional Monte Carlo [Dingec et al. \(2015\)](#).

This section serves as a user manual, guiding readers through the process of implementing PEMC for pricing an exotic option. When pricing an arithmetic Asian call option under the Heston model, the option payoff is given by:

$$P_A(\{S_t\}_t) = \max\left(\frac{1}{n_D} \sum_{i=1}^{n_D} S_{t_i} - K, 0\right)$$

where θ_{payoff} specifies the strike level K , the sampling frequency n_D and the observation dates $\{t_i\}_{i \in [n_D]}$. The Heston model is described in (2) which requires $\theta_{\text{model}} := (r, \eta, \delta, \rho, \kappa) \in \mathbb{R}^5$. For this example, let's say we use a neural network (NN) as the prediction model. Then, the PEMC framework could proceed as follows:

1. Define the parameter space Θ that encompasses realizations of

$$\theta := \underbrace{(r, \eta, \delta, \rho, \kappa, S_0, v_0, \Delta t, T)}_{\theta_{\text{model}}}, \underbrace{K, n_D}_{\theta_{\text{simulation}}}, \underbrace{\{t_i\}_{i \in [n_D]}}_{\theta_{\text{payoff}}}$$

which are of practical interest. The choice of Θ also depends on the model capacity and the model updating frequency. We shall discuss this in subsequent sections.

2. Uniformly sample θ from Θ . This step is straightforward if the parameter space is a Cartesian product of intervals. For each sampled θ , generate process $\mathbf{Y} := (S_t, v_t)_t$ using a Euler scheme with step size Δt , according to the Heston model specified by θ .
3. During the sampling of \mathbf{Y} , we collect \mathbf{X} to be the sum of Brownian increment

$$W_T^S := \sum_{j=1}^{T/\Delta t} \Delta W_{j\Delta t}^S \quad \text{and} \quad W_T^v := \sum_{j=1}^{T/\Delta t} \Delta W_{j\Delta t}^v,$$

simulated during each step of the Euler scheme. This makes the marginal of \mathbf{X} simply a two-dimensional Gaussian: $\frac{\mathbf{X}}{\sqrt{T}} \sim \mathcal{N}\left(\mathbf{0}, \begin{bmatrix} 1 & \rho \\ \rho & 1 \end{bmatrix}\right)$.

4. Save

$$\begin{aligned} \text{label} &:= \left(\frac{1}{n_D} \sum_{i=1}^{n_D} S_{t_i} - K\right)^+ \\ \text{feature} &:= (r, \eta, \delta, \rho, \kappa, S_0, \nu_0, \Delta t, T, K, n_D, \{t_i\}_{i \in [n_D]}, W_T^S, W_T^Y). \end{aligned} \quad (5)$$

5. Repeat steps 2-4 N_{train} times to generate dataset $(\text{feature}_i, \text{label}_i)_{i \in [N_{\text{train}}]}$ of size N_{train} .

6. Train a NN with weights \mathbf{w} to minimize the MSE loss:

$$\min_{\mathbf{w}} \frac{1}{N_{\text{train}}} \sum_{i \in [N_{\text{train}}]} (\text{label}_i - NN_{\mathbf{w}}(\text{feature}_i))^2$$

and use $\hat{\mathbf{w}}$ to approximate

$$NN_{\hat{\mathbf{w}}} \approx \mathbb{E} \left[\left(\frac{1}{n_D} \sum_{i=1}^{n_D} S_{t_i} - K\right)^+ \middle| r, \eta, \delta, \rho, \kappa, S_0, \nu_0, \Delta t, T, K, n_D, \{t_i\}_{i \in [n_D]}, W_T^S, W_T^Y \right].$$

7. At evaluation, a specific $\theta = (r, \eta, \delta, \rho, \kappa, S_0, \nu_0, \Delta t, T, K, n_D, \{t_i\}_{i \in [n_D]}, W_T^S, W_T^Y) \in \Theta$ is given, we generate n paired samples $(\text{label}_i, \text{feature}_i)_{i \in [n]}$ as in (5). We also generate N i.i.d. $\sqrt{T} \mathcal{N}\left(\mathbf{0}, \begin{bmatrix} 1 & \rho \\ \rho & 1 \end{bmatrix}\right)$ samples and store them as $(\text{feature}_{\tilde{j}})_{j \in [N]}$.

8. Output $PEMC := \frac{1}{n} \sum_{i=1}^n (\text{label}_i - NN_{\hat{\mathbf{w}}}(\text{feature}_i)) + \frac{1}{N} \sum_{j=1}^N NN_{\hat{\mathbf{w}}}(\text{feature}_{\tilde{j}})$

2.6. Implementation Details in PEMC

Having walked through the Asian option example under the PEMC framework, we discuss several important implementation details. These considerations are critical for successfully applying PEMC in practice.

2.6.1. Parameter Space Θ When determining the parameter space Θ , a key consideration is how frequently the model will be updated. To ensure the performance of PEMC, it is desirable that the training data encompass all practical scenarios the model is expected to encounter within the designated update period. For example, if one is calibrating a Heston

model (2) for certain SPY ETF, on a given trading day, the calibration yields a specific set of parameters: $(S_0, \nu_0, r, \eta, \delta, \rho, \kappa) = (520, 20\%, 4.5\%, 0.04, 0.3, -0.7, 0.2)$. If one updates the prediction model in PEMC once a month, then, based on historical data and market conditions, financial practitioners could make reasonable guesses about the bounds within which these parameters are likely to fluctuate over the coming month. For example, one could postulate the underlying price would mostly be fluctuating within a 5 – 6% range, i.e., around 490-550, based on the historical volatility of SPY. This expectation specifies an interval for S_0 in Θ . Similarly, one might set intervals for each parameter in the same manner, e.g., interval for $r \in (4.0\%, 5.0\%)$, anticipating that the interest rates change would not exceed half a percentage point. Finally, we note that while these parameters are jointly distributed and could be calibrated together—especially considering that many market conditions are intertwined and correlated—this is often unnecessary. Instead, one can define intervals for each parameter individually and enlarge the uncertainty set, since the coverage of practical scenarios is more important in PEMC.

This process is conceptually similar to the selection of uncertainty sets in robust optimization Ben-Tal et al. (2008) or distributionally robust optimization Esfahani and Kuhn (2018), where the goal is to include realizations of parameters with high likelihood. However, unlike robust optimization approaches, which often favor data-dependent uncertainty sets, our focus here is also guided by the expertise of financial engineers. The training parameter space is designed to reflect realistic and practical scenarios derived from domain knowledge, rather than being strictly driven by statistical guarantees. In applications, we construct reasonable Θ for practical models, such as forward curves in HJM modeling Glasserman (2013b) or local stochastic volatility 2D grids Gatheral (2006), among others.

2.6.2. The Design of X : Feature Engineering In our Asian option example, we designed the feature X as the sum of two correlated Brownian increments. As discussed in Section 2.3, the choice was motivated by two key properties:

- Predictability: The sum of Brownian motion increments explains away a large portion of the variance driving the movement of SDE.

- **Ease of Generation:** The sum of Brownian increments follows a correlated Gaussian distribution, which can be generated efficiently.

Given these reasons, it is natural to use such sums as \mathbf{X} for all related SDE driving by Brownian motion. Indeed, this is the approach we adopt in our applications, and it has proven to be both robust and effective. For cases where the path is very long, one can divide the sum into chunks of smaller increments. However, we found that using just one increment typically gives sufficient variance reduction.

However, the choice of Brownian increments, while effective, is certainly not the only one. As with most ML tasks, feature engineering that leverages domain expertise can yield better results. We illustrate with one such example, the pricing of a floating strike lookback call option, under the Heston model(2). The option payoff is given by:

$$f(\{S_t\}_t) = \max(S_T - \min_{0 \leq t \leq T} S_t, 0)$$

where S_t is the asset price process and T is the option maturity. A good choice of feature could be:

$$\mathbf{X} = (W_T^S, \min_{0 \leq t \leq T} (r - \eta/2)t + \sqrt{\eta}W_t^S).$$

The rationale behind the construction of $\min_{0 \leq t \leq T} (r - \eta/2)t + \sqrt{\eta}W_t^S$ term is grounded in the domain knowledge of the Heston model. Specifically, one who is familiar with the role of η as the mean-reverting level of variance process v_t may approximate $v_t \approx \eta$ (i.e., assume fixed volatility) and simplify the asset price process to a geometric Brownian motion:

$$S_t \approx S_0 e^{(r-\eta/2)t + \sqrt{\eta}W_t^S} \text{ and } \min_{0 \leq t \leq T} S_t \approx S_0 e^{\min_{0 \leq t \leq T} (r-\eta/2)t + \sqrt{\eta}W_t^S}.$$

This approximation leads to the expression: $f(\{S_t\}_t) \approx S_0 e^{(r-\nu/2)T + \sqrt{\nu}[X]_1} - S_0 e^{[X]_2}$, which could serve as a potentially effective approximation of $f(\{S_t\}_t)$. This corresponds directly to Property 1 in the construction of \mathbf{X} in 2.3. For Property 2, the marginal distribution of \mathbf{X} permits efficient and parallelizable simulation. In particular, applying Girsanov's Theorem enables one to derive a closed-form expression for the joint density of $([X]_1, [X]_2)$ Karatzas and Shreve (1991). This result makes it straightforward to sample these components directly.

2.6.3. Eliminating Data Storage Overheads In typical ML workflows, training datasets—often costly, scarce, and carefully curated—are stored and reused extensively. By contrast, within the PEMC framework, the nature of data generation during the prediction model training in Algorithm 1, actually does not require extensive data storage. This difference stems from two main considerations.

First, the volume of training data required to achieve a well-performing prediction model can be large. Storing all of it would be both expensive and unnecessary. In PEMC, the training data can be produced directly via Monte Carlo simulation, ensuring an effectively unlimited supply. Second, this flexibility allows for a more efficient workflow. Data can be generated “on the fly” and processed in streaming fashion. For example, to train on a large number of N_{train} samples, one could iteratively produce small batches, train the model on these batches, and discard them after training. In this manner, we have successfully trained models in the applications using data on the order of 10^7 – 10^8 .

3. Analysis and Performance

In this section, we provide a detailed and comprehensive analysis of the PEMC estimator, presenting both theoretical results and practical considerations. All properties of PEMC discussed here pertain to the evaluation stage, where θ is fixed. Henceforth, we omit the explicit dependence on θ in the notation (e.g., writing \mathbf{Y} in place of $\mathbf{Y}(\theta)$). We begin by establishing the unbiasedness of our estimator.

3.1. Bias Analysis

THEOREM 1 (Unbiasedness). *The PEMC estimator in equation (4), is unbiased:*

$$\mathbb{E} \left[\frac{1}{n} \sum_{i=1}^n (f(\mathbf{Y}_i) - g(\mathbf{X}_i)) + \frac{1}{N} \sum_{j=1}^N g(\tilde{\mathbf{X}}_j) \right] = \mathbb{E}[f(\mathbf{Y})]$$

Proof First note that g is pre-trained. The proof then follows since \mathbf{X}_i and $\tilde{\mathbf{X}}_j$ have the same marginal distribution for any i, j . \square

Given the unbiased nature of PEMC, the analysis of PEMC as a Monte Carlo method primarily hinges on its variances and computational costs.

3.2. Variance Analysis

To facilitate the analysis, we first introduce some necessary notation.

DEFINITION 1. Given function f that takes input \mathbf{Y} and g that takes input \mathbf{X} (so both f, g are considered fixed here), we denote

$$\sigma_{f-g}^2 := \text{Var}(f(\mathbf{Y}) - g(\mathbf{X})), \quad \sigma_f^2 := \text{Var}(f(\mathbf{Y})), \quad \text{and} \quad \sigma_g^2 := \text{Var}(g(\mathbf{X})).$$

Similarly, we denote cost of generating a coupled sample $f(\mathbf{Y}) - g(\mathbf{X})$ as c_{f-g} , the cost of generating $f(\mathbf{Y})$ as c_f and the cost of generating $g(\mathbf{X})$ as c_g .

LEMMA 1. Using the notations from 1, we have

$$\text{Cov}(f(\mathbf{Y}), g(\mathbf{X})) = \frac{\sigma_f^2 + \sigma_g^2 - \sigma_{f-g}^2}{2}.$$

We make two remarks here. First, since we generally obtain \mathbf{X} in the same process during the generation of \mathbf{Y} , thus typically in either sense of the cost, we have $c_{f-g} \approx c_f$. Second, the term cost is intentionally left ambiguous because its interpretation varies depending on the context. In some cases, cost refers to the sample size, while in others it represents the wall-clock time required to generate and evaluate the sample. Furthermore, in certain scenarios, both time and computational resources must be jointly considered and optimized, under parallelization and other speedup, making the concept of cost more instance dependent. Therefore, for now, we use cost as an umbrella term to capture various meanings under different contexts.

LEMMA 2. The Variance of the PEMC estimator in equation (4) is

$$\text{Var}(PEMC) = \frac{1}{n} \sigma_{f-g}^2 + \frac{1}{N} \sigma_g^2.$$

Proof First note that g is pre-trained. Moreover, in the evaluation phase, data $(\mathbf{Y}_i, \mathbf{X}_i)_{i \in [n]}$ are generated independent of $(\tilde{\mathbf{X}}_j)_{j \in [N]}$. \square

Having established the unbiasedness and the variance form of the PEMC estimator, we could turn to inference. In particular, using consistent estimates of variance, the application of the central limit theorem enables the construction of valid asymptotic confidence intervals. Moreover, a range of inferential techniques may be employed—such as deriving high-probability bounds or other non-asymptotic guarantees—the asymptotic confidence interval construction suffices to illustrate the point. The approach follows closely from results in prediction-powered inference [Angelopoulos et al. \(2023\)](#).

THEOREM 2 (Asymptotic Confidence Intervals). *In the set up of the evaluation algorithm 2, given the prediction model g , $(\mathbf{Y}_i, \mathbf{X}_i)_{i \in [n]}$ and $(\tilde{\mathbf{X}}_j)_{j \in [N]}$, we define*

$$\hat{\sigma}_{f-g}^2 = \frac{1}{n} \sum_{i=1}^n \left(f(\mathbf{Y}_i) - g(\mathbf{X}_i) - \left(\frac{1}{n} \sum_{i'=1}^n f(\mathbf{Y}_{i'}) - g(\mathbf{X}_{i'}) \right) \right)^2,$$

and

$$\hat{\sigma}_g^2 = \frac{1}{N} \sum_{j=1}^N \left(g(\tilde{\mathbf{X}}_j) - \frac{1}{N} \sum_{j'=1}^N g(\tilde{\mathbf{X}}_{j'}) \right)^2,$$

be the respective sample variance. Let $z_{1-\alpha/2}$ denote the $(1 - \alpha/2)$ -quantile of the standard normal distribution. Then, the interval

$$\left(PEMC - z_{1-\alpha/2} \sqrt{\frac{\hat{\sigma}_{f-g}^2}{n} + \frac{\hat{\sigma}_g^2}{N}}, \quad PEMC + z_{1-\alpha/2} \sqrt{\frac{\hat{\sigma}_{f-g}^2}{n} + \frac{\hat{\sigma}_g^2}{N}} \right),$$

is an asymptotically valid $1 - \alpha$ confidence interval for $\mathbb{E}[f(\mathbf{Y})]$, as $n, N \rightarrow \infty$.

Proof Theorem 1 establishes PEMC is unbiased. Moreover, $\hat{\sigma}_{f-g}^2, \hat{\sigma}_g^2$ are consistent estimates of $\sigma_{f-g}^2, \sigma_g^2$, the results follows from Lemma 2 and the central limit theorem and Slutsky's theorem. \square

3.3. Variance Reduction

Having analyzed the bias and variance of the PEMC estimator, we now turn to a fundamental practical question: Under a fixed cost budget—whether measured in terms of the number of samples, computational time, or other limited resources—when does PEMC outperform

standard Monte Carlo (MC)? Our aim is to understand how PEMC's variance reduction scales with its cost, thereby identifying regimes where PEMC emerges as more efficient than standard MC. To this end, we first determine the optimal allocation of the sample sizes n (the number of expensive full simulations) and N (the number of cheap, feature-only evaluations) within the PEMC framework, given a total resource budget B . This investigation provides a guideline for parameter selection and reveals conditions under which PEMC's gains are maximized.

LEMMA 3. *Assuming $n, N \in \mathbb{R}^+$ and $c_g, c_{f-g} \in \mathbb{R}^+$, the optimal allocation between n and N for PEMC, for any positive budget B , follows as*

$$\frac{n}{N} = \frac{\sigma_{f-g}}{\sigma_g} \cdot \sqrt{\frac{c_g}{c_{f-g}}} . \quad (6)$$

Proof By relaxing the constraints to $n, N \in \mathbb{R}^+$, the optimization problem

$$\begin{aligned} \min_{n>0, N>0} \quad & \frac{1}{n} \sigma_{f-g}^2 + \frac{1}{N} \sigma_g^2 . \\ \text{s.t.} \quad & n c_{f-g} + N c_g \leq B . \end{aligned}$$

is jointly convex in $n, N \in \mathbb{R}^+$. The objective value also approaches infinity as $N \rightarrow 0$ or $n \rightarrow 0$. Consequently, the strict convexity ensures the existence of a global minimizer in the interior and directly solving the Lagrangian gives us the result. \square

In practice, $c_{f-g} \gg c_g$ often holds which suggests one should set $N \gg n$ according to Lemma 3. While Lemma 3 relies on treating $n, N \in \mathbb{R}^+$ as continuous—ignoring the integer constraints $n, N \in \mathbb{N}^+$ —this continuous approximation still provides valuable guidance when $n, N \geq 1$. In fact, in practice, we found the ratio suggested by Lemma 3 guides near-optimal parameter selection. However, the standard MC corresponds to the case $N = 0$, a scenario not covered by Lemma 3, and thus requires separate consideration. Building on Lemma 3, we can estimate an upper bound on the variance reduction PEMC can achieve relative to standard MC under these idealized assumptions.

LEMMA 4. Assume $c_{f-g} = c_f$. In the same setup as Lemma 3, the variance ratio between PEMC under the optimal allocation and standard MC follows as

$$\frac{\text{Var}(PEMC)}{\text{Var}(MC)} = \frac{\sigma_{f-g}^2}{\sigma_f^2} \left(1 + \frac{\sigma_g}{\sigma_{f-g}} \cdot \sqrt{\frac{c_g}{c_f}} \right) + \frac{\sigma_g^2}{\sigma_f^2} \left(\frac{\sigma_{f-g}}{\sigma_g} \cdot \sqrt{\frac{c_g}{c_f}} + \frac{c_g}{c_f} \right). \quad (7)$$

Proof Based on the results of Lemma 3, we can deduce that this ratio again does not depend on the budget B , so we omit its dependence in the statement. Moreover, we can conveniently choose a budget of the form $B = n_0 c_{f-g} + n_0 \frac{\sigma_g}{\sigma_{f-g}} \cdot \sqrt{\frac{c_{f-g}}{c_g}} c_g$ which gives an allocation of $n = n_0$ and $N = n_0 \frac{\sigma_g}{\sigma_{f-g}} \cdot \sqrt{\frac{c_{f-g}}{c_g}}$ for PEMC in accordance with Lemma 3, while comparing with B/c_f samples for standard MC. The rest follows from Lemma 2 and the assumption $c_f = c_{f-g}$. \square

At this point, a natural question arises: how can we gauge $\frac{\sigma_{f-g}^2}{\sigma_f^2}$ or $\frac{\sigma_g^2}{\sigma_f^2}$ in practice? How are these ratios tied to the quality of the predictive model g in PEMC? As we shall see, the extent of variance reduction that PEMC can deliver is linked to how well g is trained. To illustrate this, we first consider an ideal scenario where g is trained to the optimum, i.e., the true regression function.

LEMMA 5. Suppose $c_{f-g} = c_f$, $f(\mathbf{Y})$ is square-integrable and $g = \mathbb{E}[f(\mathbf{Y}) | \mathbf{X}]$. Define $\rho := \text{corr}(f, g)$ and $c := \frac{c_g}{c_f}$. Then we have $\rho = \frac{\sigma_g}{\sigma_f}$ and the $\frac{\text{Var}(PEMC)}{\text{Var}(MC)}$ in Lemma 4 becomes

$$r(\rho, c) := (1 - \rho^2) \left(1 + \frac{\rho}{\sqrt{1 - \rho^2}} \cdot \sqrt{c} \right) + \rho^2 \left(\frac{\sqrt{1 - \rho^2}}{\rho} \cdot \sqrt{c} + c \right). \quad (8)$$

Proof When $g = \mathbb{E}[f(\mathbf{Y}) | \mathbf{X}]$ is the true regressor, i.e.,

$$g = \arg \min_{h \text{ measurable}} \mathbb{E}[(f(\mathbf{Y}) - h(\mathbf{X}))^2],$$

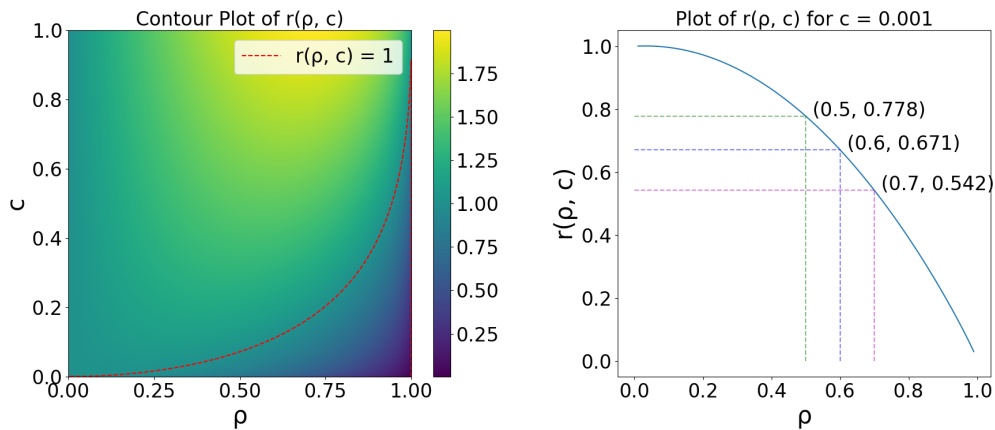
and f is square-integrable, it follows that $\mathbb{E}[(f - g)h(\mathbf{X})] = 0$ for all square-integrable h . Plug in $h = g$, we obtain $\text{Cov}(f - g, g) = 0$. Consequently we have $\rho := \text{corr}(f, g) = \frac{\sigma_g}{\sigma_f}$ and $\sigma_f^2 = \sigma_{f-g}^2 + \sigma_g^2$, which further implies $\sigma_g = \rho \sigma_f$ and $\sigma_{f-g}^2 = (1 - \rho^2) \sigma_f^2$. The rest follows from $c_{f-g} = c_f$. \square

Lemma 5 says that the variance reduction of PEMC relative to standard MC can be approximated by the function $r(\rho, c)$ in (8), where $\rho = \sigma_g/\sigma_f$ captures the predictive power of $g(\mathbf{X})$ for $f(\mathbf{Y})$, and $c = c_g/c_f$ quantifies the relative cost of evaluating $g(\mathbf{X})$ versus generating full samples for $f(\mathbf{Y})$. In Figure 1, we visualize the variance reduction function $r(\rho, c)$ for $\rho, c \in (0, 1)$. On the left is a contour plot of $r(\rho, c)$ where the red line traces the curve $r(\rho, c) = 1$, corresponding to the “break-even” boundary where PEMC’s variance matches that of MC. Regions below this line, $\{(\rho, r) \in [0, 1]^2 | r(\rho, c) < 1\}$, represent regimes of ρ and c where PEMC achieves variance reduction, i.e., where ρ is sufficiently large and c is sufficiently small. On the right, the graph of $r(\rho, c)$ as a function of ρ when $c = 0.001$ provides a clear benchmark: a correlation $\rho = 0.5$ yields approximately 22.2% variance reduction, while $\rho = 0.7$ yields about 45.8%. In our PEMC applications, we design feature \mathbf{X} and predictive model g so that, for most $\theta \in \Theta$ during evaluation, we can safely gauge that c falls between 10^{-2} to 10^{-3} and ρ exceeds 0.5. In these regions, Lemma 3 suggests choosing N/n in the range of 5 to 20 for near-optimal performance. In our experiments, a ratio of $N = 10n$ proved effective.

3.3.1. Learning Theory Estimates The statements in Lemma 3 assume that g represents the true regression function $\mathbb{E}[f|\mathbf{X}]$. In practice, however, g is obtained through a learning procedure applied to finite training samples, and thus will only approximate the true conditional expectation. Consequently, any practical implementation of PEMC must account for the approximation and estimation errors inherent in the training process. Moreover, as the parameter θ varies, the correlation ρ between $g(\mathbf{X})$ and $f(\mathbf{Y})$, the complexity of the underlying model and payoff function also changes.

To rigorously quantify these effects, one can invoke tools from statistical learning theory, such as uniform convergence bounds, VC-dimension, or Rademacher complexities (Vapnik 1998, Bartlett and Mendelson 2005, Mohri et al. 2018). These quantities, by relating the complexity of the function class used to represent g and the available training sample size N_{train} , lead to error bounds that ensure, with high probability, that the trained predictor g is

Figure 1 Variance Reduction Function $r(\rho, c)$.



Note. Left figure: A contour map of the variance reduction ratio $r(\rho, c)$ as a function of the correlation $\rho = \sigma_g/\sigma_f$ and relative cost $c = c_g/c_f$. The red curve indicates the curve $r(\rho, c) = 1$ and the regimes where PEMC attains variance reduction over MC lie below the line. Right figure: A graph of $r(\rho, c)$ as a function of ρ when $c = 10^{-3}$.

close to the true regression function within a controlled margin. Although numerous, more refined approaches exist, we avoid delving deeply into them so as not to distract from our main theme. Instead, we adopt a standard, off-the-shelf, almost ‘placeholder’-type result detailed in the Appendix, that illustrates the typical form of guarantees one could expect from PEMC.

LEMMA 6. *Under the regularity conditions specified in the Appendix, for any $\epsilon, \delta > 0$, there exists a sufficiently large sample size N_{train} and a suitably chosen neural network class from which we select and train a predictor g on N_{train} samples, such that*

$$\frac{\text{Var}(PEMC)}{\text{Var}(MC)} \leq r(\rho, c) + \epsilon$$

for a randomly evaluated $\theta \sim \Theta$ with probability at least $1 - \delta$.

The simplified version captures the essential idea: under suitable regularity conditions, one can achieve the result of Lemma 3 within an arbitrarily small margin, as both the sample size N_{train} and the complexity of the hypothesis class increase.

3.4. Control Variate Coefficient

In this section we explore a connection between the PEMC framework and traditional Control Variate (CV) methods. In (4), note that we could introduce a free parameter a to create a variant:

$$PEMC(a) := \frac{1}{n} \sum_{i=1}^n (f(\mathbf{Y}_i) - ag(\mathbf{X}_i)) + \frac{1}{N} \sum_{j=1}^N ag(\tilde{\mathbf{X}}_j) \quad (9)$$

The introduction of a is analogous to CV approaches, where the parameter a is chosen to minimize variance. In PEMC, this viewpoint may appear somewhat redundant since ag is also a valid prediction model, which suggests a would be chosen implicitly during the training of the prediction model. Nevertheless, suppose g is fixed. Then $\frac{1}{n} \sum_{i=1}^n -g(\mathbf{X}_i) + \frac{1}{N} \sum_{j=1}^N g(\tilde{\mathbf{X}}_j)$ can be viewed as a readily available, zero-mean control variate. We can then choose a which minimizes the variance. The optimal a^* then is:

$$a^* = \frac{\text{Cov}(f(\mathbf{Y}), g(\mathbf{X}))}{(n/N + 1)\text{Var}(g(\mathbf{X}))}.$$

In the ideal scenario, we have $N \gg n$ and $g(\mathbf{X}) = \mathbb{E}[f(\mathbf{Y})|\mathbf{X}]$, which would imply $\text{Cov}(f(\mathbf{Y}) - g(\mathbf{X}), g(\mathbf{X})) = 0$ and $\text{Cov}(f(\mathbf{Y}), g(\mathbf{X})) = \text{Var}(g(\mathbf{X}))$. This would further imply $a^* = \frac{1}{1+n/N} \approx 1$. Consequently, we can justify PEMC's default choice of $a = 1$, which saves us the trouble of estimating a^* , and gives PEMC a degree of robustness.

3.5. Variance Reduction of PEMC: An Example on Asian Options

We revisit the Asian option example and conduct experiments using the arithmetic Asian call option under the Geometric Brownian Motion (GBM) model. We choose the GBM model instead of the Heston model (2) to facilitate a direct comparison between PEMC, standard Monte Carlo (MC), and the traditional Control Variate (CV) method on the extent of variance reduction. This is because the geometric Asian option, which serves as a well-established control variate, is analytically tractable within the GBM framework but lacks a closed-form solution under the Heston model (Dingec et al. 2015).

This experiment aims to demonstrate the typical level of variance reduction that PEMC achieves. Our focus is strictly limited to variance reduction, because the GBM model actually allows for highly efficient and parallelized generation of both asset paths and corresponding payoffs, making the simulation of Y computationally straightforward. In other words, one could not fully leverage PEMC's strengths in GBM model and this toy experiment only serves to provide insights into PEMC's effectiveness in a controlled setting where a known CV exists. Practical applications and actual use-cases of PEMC will be provided in Section 4.

3.5.1. Experimental Setup We implement the PEMC procedure detailed in Section 2.5, utilizing a neural network (NN) as the predictive model. The asset price follows the Geometric Brownian Motion (GBM) model:

$$dS_t = rS_t dt + \sigma S_t dW_t^S. \quad (10)$$

The payoff calculation $P_A(\{S_t\}_t) = (\frac{1}{n_D} \sum_{i=1}^{n_D} S_{t_i} - K, 0)^+$ with $n_D = 252$, where simulations are carried out using daily time increments (i.e., $\Delta t = 1$). The parameter space $\theta := (r, S_0, \sigma, K) \in \Theta$ is: $r \in [0.01, 0.03]$, $S_0 \in [80, 120]$, $\sigma \in [0.05, 0.25]$, and $K \in [90, 110]$. For our feature X , we experiment with the whole sum of Brownian increments $W_T^S := \sum_{j=1}^{252} \Delta W_j^S$ with $\dim(X) = 1$. We also tried a more granular representation where we partition 252 Brownian increments evenly into 14 parts, each summing 18 consecutive increments: $[X]_i = \sum_{j=18(i-1)+1}^{18i} \Delta W_j^S$ for $i \in [14]$, yielding $\dim(X) = 14$. The neural network is trained on a dataset comprising $N_{\text{train}} = 1.28 \times 10^6$ samples, generated by uniformly sampling $\theta \sim \Theta$.

The neural network architecture consists of three components: a θ network branch, a X network branch, and a combined network. This architecture incorporates several modern deep learning practices, including Batch Normalization (Ioffe and Szegedy 2015), Rectified Linear Unit (ReLU) activations (Nair and Hinton 2010), and skip connections (He et al. 2016) to enhance training stability and model performance. The θ network

branch processes the 4-dimensional input θ using two fully connected layers with Batch Normalization and ReLU activation functions, outputting a 10-dimensional feature vector for subsequent processing. The X network branch uses two fully connected layers with width $\max(32, 2 \dim(X))$ neurons. Finally, the combined network integrates outputs from both branches through concatenation and employs skip connections featured in ResNet architectures to preserve information flow. The concatenated features pass through two additional fully connected layers with Batch Normalization and ReLU activation to produce the final prediction for PEMC. The network is implemented using PyTorch (Paszke et al. 2019) and trained using the Adam optimizer (Kingma and Ba 2014) with a learning rate of 1×10^{-3} , incorporating dropout layers (Srivastava et al. 2014) with a rate of 0.5 after each hidden layer to prevent overfitting.

3.5.2. Evaluation For comparison, we implement PEMC, MC and CV method with geometric Asian option

$$P_G(\{S_t\}_t) = \left(\left(\prod_{i=1}^{n_D} S_{t_i} \right)^{\frac{1}{n_D}} - K, 0 \right)^+,$$

for the evaluation at $\theta = (r, S_0, \sigma, K) = (0.02, 100, 0.2, 100)$. The CV estimator is given by

$$\text{CV} = \frac{1}{n} \sum_{i=1}^n \left(P_A(\{S_t^{(i)}\}_t) - P_G(\{S_t^{(i)}\}_t) \right) + P_G^{\text{exact}}(\theta),$$

where $P_G^{\text{exact}}(\theta)$ is the closed-form price of geometric Asian option (with correction regarding n_D) (Glasserman 2013b). We first evaluate the mean of 2×10^9 MC samples as the ground truth value A_0 . Then, we evaluate n sample average of the MC, PEMC ($N = 10n$) and the geometric CV estimator for $n = 1000, 4000, 9000$ respectively, to record 3 different estimator for A_0 . Then we repeat the experiments 300 times to get 300 estimators for each $n \in \{1000, 4000, 9000\}$ and each method in {MC, PEMC, Geometric CV}, to compare against A_0 . The performance of the estimators is summarized in Table 11 and Figure 2.

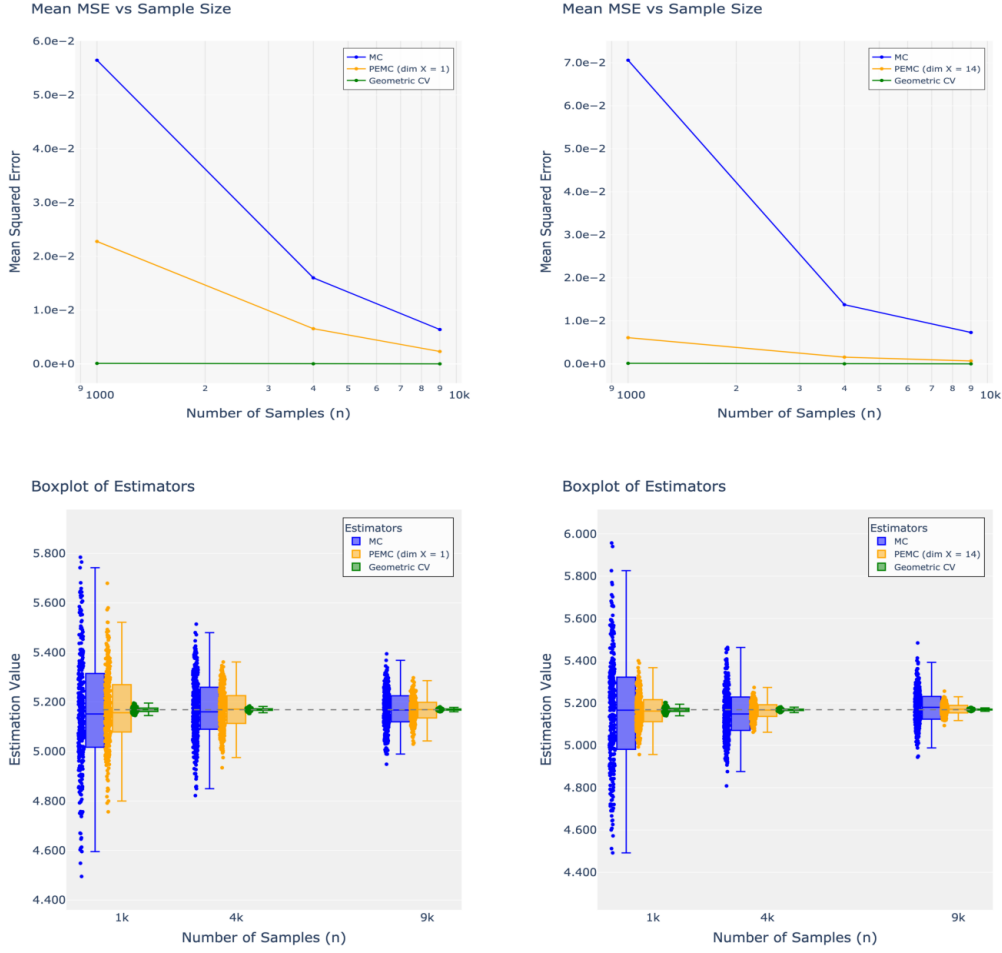
Given that all estimators are unbiased, our analysis focuses exclusively on variance-related metrics. The experimental results demonstrate the superior performance of the

Table 1 Root Mean Squared Error from 300 Experiments

Method	$n = 1000$	$n = 4000$	$n = 9000$
Monte Carlo (MC)	0.2376	0.1173	0.0854
PEMC (dim $X = 1$)	0.1509	0.0809	0.0481
PEMC (dim $X = 14$)	0.0781	0.0397	0.0261
Geometric CV	0.0099	0.0051	0.0036

PEMC framework compared to the standard Monte Carlo (MC) estimator. In particular, in all sample sizes, the PEMC framework delivers visible variance reduction over MC: PEMC’s basic variant with $\dim X = 1$ achieves a 30-40% reduction in root mean squared error (RMSE) relative to MC, while the more sophisticated variant with $\dim X = 14$ attains an impressive 65-70% reduction in RMSE over MC. However, the Geometric CV emerges as the most efficient estimator by far, with RMSE an order of magnitude smaller than MC.

To better understand this hierarchy in estimator performance, it is helpful to recognize PEMC not as a specific estimator, but rather as a framework that latches on and enhance an existing baseline. In our current example, we chose standard MC as the baseline, and design our PEMC directly upon MC to improve it. This also illustrates a common state of practice: in most complex scenarios, sophisticated baselines like CV are not available, and practitioners must rely on some variants of naive MC methods. Then, PEMC can be applied to these baselines to achieve variance reduction. However, PEMC is a flexible framework designed to enhance general simulation baselines, including sophisticated ones, not just standard Monte Carlo. In particular, when a control variate method is available, such as in our current example, PEMC can be built upon it to potentially achieve even greater variance reduction. To see how, in Algorithm 1, we change the label from $P_A(\{S_t\}_t)$ (MC baseline) to $P_A(\{S_t\}_t) - P_G(\{S_t\}_t) + P_G^{\text{exact}}(\theta)$ (Geometric CV baseline), and let the model g learn

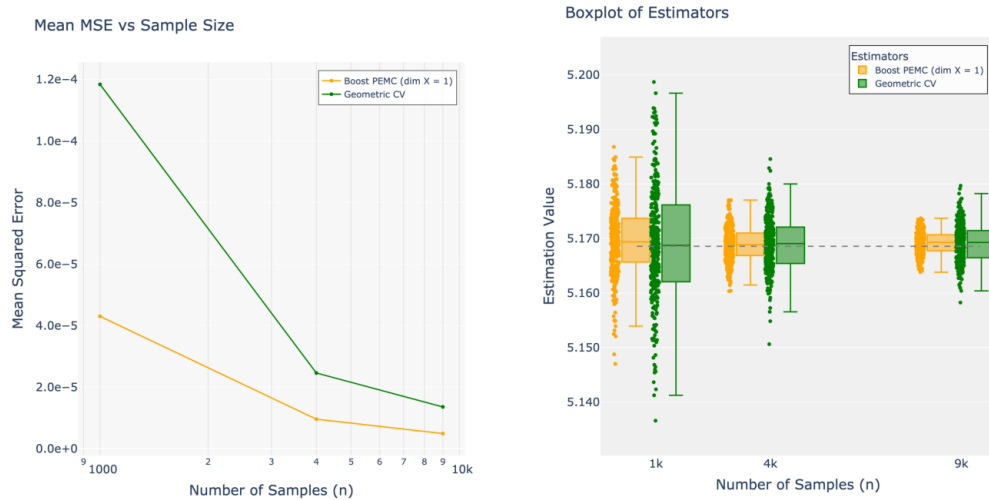
Figure 2 Performance of Estimators for Asian Options.

Note. Comparison of estimator across Monte Carlo (MC), PEMC, and Geometric Control Variate (CV) based on 300 experiments. Top: Mean squared errors (MSE) plot as a function of n for (left) PEMC with $\dim X = 1$ and (right) PEMC with $\dim X = 14$, both compared against MC and Geometric CV. Bottom: Corresponding boxplots of the 300 estimates.

$$\begin{aligned}
 g(\boldsymbol{\theta}, \mathbf{X}(\boldsymbol{\theta})) &\approx \mathbb{E}_{\text{risk neutral measure}(\boldsymbol{\theta})} \left[P_A(\{S_t\}_t) - P_G(\{S_t\}_t) + P_G^{\text{exact}}(\boldsymbol{\theta}) \middle| (\boldsymbol{\theta}, \mathbf{X}(\boldsymbol{\theta})) \right] \\
 &= \mathbb{E}_{\text{risk neutral measure}(\boldsymbol{\theta})} \left[P_A(\{S_t\}_t) - P_G(\{S_t\}_t) \middle| (\boldsymbol{\theta}, \mathbf{X}(\boldsymbol{\theta})) \right] + P_G^{\text{exact}}(\boldsymbol{\theta}). \quad (11)
 \end{aligned}$$

This formulation suggests we can train g on the difference of $P_A(\{S_t\}_t) - P_G(\{S_t\}_t)$ as labels and then add back the closed-form $P_G^{\text{exact}}(\boldsymbol{\theta})$ to g . We implemented this approach,

Figure 3 Performance of CV-based Estimators for Asian Options.



Note. Comparison of estimator performance for Boost PEMC and Geometric Control Variate (CV) based on 300 experiments. Left: Mean squared errors (MSE) plot as a function of n . Right: Corresponding boxplots of 300 estimates.

which we call “Boost PEMC,” using the basic PEMC variant where $X = W_T^S := \sum_{j=1}^{252} \Delta W_j^S$ with $\dim X = 1$. As shown in Table 2 and Figure 3, this Boost PEMC indeed achieves variance reduction over the sophisticated Geometric CV estimator, delivering a 35-40% reduction in RMSE, remarkably consistent with the relative performance gain we observed when applying PEMC to the MC baseline in Figure 2.

Table 2 Root Mean Squared Error from 300 Experiments

Method	$n = 1000$	$n = 4000$	$n = 9000$
Boost PEMC ($\dim X = 1$)	0.0065	0.0031	0.0021
Geometric CV	0.0099	0.0051	0.0036

This experiment with Asian options under the GBM model serves as a controlled study to demonstrate PEMC’s effectiveness as a variance reduction framework. In the following section, we go beyond this over-simplified setting and apply PEMC to practical applications in complex derivative pricing.

4. Applications

After establishing the theoretical foundations of PEMC and demonstrating its effectiveness in controlled environments, we now apply it to real-world financial scenarios where the complexity of models often renders standard variance reduction techniques difficult or unavailable. In this section, we examine PEMC in practice through two complex pricing problems. In particular, we examine variance swaps pricing under stochastic (local) volatility models (Dupire et al. 1994, Derman and Kani 1994, Gatheral 2006), and the pricing of swaptions under the Heath-Jarrow-Morton (HJM) framework (Carmona 2007). In both cases, the path-dependent nature of the contracts and the complexity of the model dynamics make traditional control variates difficult.

4.1. Variance Swaps Pricing

Variance swaps are financial derivatives that enable investors to trade future realized volatility against current implied volatility (Bayer et al. 1999). Unlike traditional options, which derive their value from the underlying asset's price, variance swaps are based on the variance of the asset's returns over a specified period (Derman and Fantazzini 1999). This unique structure allows for pure exposure to volatility, making variance swaps valuable tools for risk management and speculative strategies (Gatheral 2006, Protter 2010).

In this subsection, we present an application of the PEMC framework in pricing a variance swaps, with the underlying asset paths assumed to be generated according to a Heston model (2) and a Stochastic Local Volatility (SLV) model (Ren et al. 2007), respectively. These models represent two distinct approaches to stochastic volatility modeling in practical derivatives pricing: the Heston model offers a parsimonious parametric form with relatively few parameters to calibrate, while the SLV model provides greater flexibility through a data-intensive, non-parametric specification of the volatility surface. By examining both cases, we demonstrate PEMC's versatility across the spectrum of model complexity.

4.1.1. Variance swaps under a Heston model Under the Heston model (2), and the procedure follows from the illustration in Section 2.5. Given $\theta_{\text{model}} := (r, \kappa, \eta, \delta, \rho)$, the asset price $\{S_t\}_t$ is simulated by Euler's scheme with fixed T and Δt :

$$\begin{aligned} v_{t+\Delta t} &\leftarrow \kappa(\eta - v_t)\Delta t + \delta\sqrt{v_t}\Delta W_t^v, \\ S_{t+\Delta t} &\leftarrow S_t \exp\left(\left(r - \frac{1}{2}v_{t+\Delta t}\right)\Delta t + \sqrt{v_{t+\Delta t}}\Delta W_t^S\right). \end{aligned}$$

where $(\Delta W_t^S, \Delta W_t^v) \stackrel{\text{i.i.d.}}{\sim} \sqrt{\Delta t} \cdot \mathcal{N}\left(\mathbf{0}, \begin{bmatrix} 1 & \rho \\ \rho & 1 \end{bmatrix}\right)$. For each asset path $\{S_t\}_t$, the payoff is

$$f_{\theta_{\text{payoff}}}(\{S_t\}_t) := \sqrt{\frac{252 \times \sum_{t=1}^{T/\Delta t} \log(S_t/S_{t-1})^2}{T/\Delta t}} - K. \quad (12)$$

Note that due to the linear form of strike K in the payoff, it suffices to effectively removes strike K from training. We also conveniently omit any discount factor. The parameters space Θ , as well as the evaluation θ , is summarized in Table 4.

Table 3 Parameter Setup in Heston Model

mode	S_0	r	v_0	κ	η	δ	ρ	$T, \Delta t$
$N_{\text{train}} = 3,000,000$	[50, 150]	[0.01, 0.05]	[0.1, 0.375] ²	[1.5, 4.5]	[0.1, 0.3] ²	[0.1, 1.0]	[-0.2, -0.9]	
evaluation	100	0.02	0.25 ²	3.0	0.2 ²	0.6	-0.4	1, 1/252

The feature \mathbf{X} is constructed by

$$W_T^S := \sum_{j=1}^{T/\Delta t} \Delta W_{j\Delta t}^S \quad \text{and} \quad W_T^v := \sum_{j=1}^{T/\Delta t} \Delta W_{j\Delta t}^v,$$

which are jointly distributed as $\sqrt{T} \cdot \mathcal{N}(0, \begin{bmatrix} 1 & \rho \\ \rho & 1 \end{bmatrix})$ just as in Section 2.5. For the prediction model training in PEMC algorithm 1, a basic Residual Network (ResNet)-style architecture (He et al. 2016) is adopted and trained on $N_{\text{train}} = 3 \times 10^6$ samples. The network consists of two Multi-Layer Perceptron (MLP) blocks connected through skip connections. The first MLP block processes (θ, \mathbf{X}) together and pass them through hidden layers with dimension 512, eventually producing a 256-dimensional intermediate representation. This output is then fed into the second MLP block, which maintains the same hidden dimension of

256 throughout its layers. The complete architecture specification is provided in Table 4. At evaluation stage (i.e., Algorithm 2), we use θ in Table 4 and set $N = 10n$ as before. Following our evaluation methodology from Section 3.5, we first establish a ground truth

Table 4 Hyper-parameter Setup for Neural Network

1st MLP block	2nd MLP Block
hidden dim: 512; output dim: 256	hidden dim: 256

value by averaging 5×10^7 MC samples. We then implement both standard MC and PEMC estimators (with $N = 10n$) using sample sizes $n \in \{1000, 2000, 4000, 8000, 10000, 20000\}$, repeating each experiment 200 times to assess sampling variability. As shown in Table 5, PEMC achieves a 30-50% reduction in root mean squared error compared to standard MC, consistent with the variance reduction levels we observed in Section 3.5. This demonstrates that PEMC’s effectiveness as a variance reduction technique carries over to more complex models and derivative products.

Table 5 RMSE from 200 Experiments for Pricing Variance Swap under the Heston Model

Method	$n = 1000$	$n = 2000$	$n = 4000$	$n = 6000$	$n = 8000$	$n = 10000$	$n = 20000$
Monte Carlo (MC)	0.0996	0.0659	0.0517	0.0391	0.0366	0.0290	0.0218
PEMC	0.0599	0.0387	0.0263	0.0233	0.0213	0.0179	0.0126

4.1.2. Variance swaps under an SLV model Having demonstrated PEMC’s effectiveness for the Heston model in Section 4.1.1, we turn to the more sophisticated Stochastic Local Volatility (SLV) framework. While parametric models like Heston offer mathematical elegance and computational efficiency, they often lack the flexibility to fully capture market dynamics (Gatheral 2006). SLV models emerged as a hybrid approach that combines the market-implied local volatility surface with stochastic volatility dynamics (Guyon and Henry-Labordère 2014), providing practitioners with greater calibration flexibility and more accurate price reproduction across strike-maturity ranges (Ren et al. 2007).

The increased modeling power of SLV, however, comes with significant computational challenges. It is known that SLV has no closed-form formula for even vanilla options (Tataru and Fisher 2010). Moreover, unlike the Heston model's parsimonious parameter set, SLV requires handling a full volatility surface discretized on a dense 2D grid, effectively turning our parameter space Θ for PEMC into a high-dimensional object. To efficiently process this grid-structured volatility data, we adopt a Convolutional Neural Network (CNN) architecture (LeCun et al. 1998) for our PEMC implementation, effectively feeding the local volatility surface as an image into PEMC. The CNNs are particularly well-suited for this task as they naturally exploit the spatial relationships in the volatility surface, similar to their success in image processing tasks (He et al. 2016, Krizhevsky et al. 2012).

Under the SLV model, we adopt the following SDEs for simulating the asset price $\{S_t\}_t$:

$$dS_t = rS_t dt + \sigma(S_t, t)e^{\nu_t} S_t dW_t^S, \quad (13)$$

$$d\nu_t = \kappa(\eta_t - \nu_t)dt + \delta dW_t^\nu, \quad (14)$$

with $\langle dW_t^S, dW_t^\nu \rangle = \rho$ and $\eta_t := -\frac{\delta^2}{2\kappa}(1 + e^{-2\kappa t})$. Here $\sigma(\cdot, \cdot) : \mathbb{R} \times \mathbb{R}^+ \rightarrow \mathbb{R}^+$ is 2D function representing the local volatility surface and $\exp(\nu_t)$ is a stochastic multiplier with $\exp(\nu_0) = 1$ and $\mathbb{E}[e^{2\nu_t}] = 1$. In practice, local volatility surfaces are calibrated to and stored as discrete two-dimensional grids indexed by asset prices (spot) and time. During simulation, these discrete values are interpolated as needed to obtain volatilities at arbitrary price-time points (Coleman et al. 2001). For our PEMC implementation, we treat this discrete grid as part of our input parameter θ_{model} , reflecting how the market-calibrated surfaces would be used in practice. While local volatility models (Dupire et al. 1994, Derman and Kani 1994) and their calibration to market data constitute an extensive research area in their own right, our focus here is on the PEMC implementation where, a calibrated local volatility has been given for evaluation, regardless of the calibration method used to obtain it.

Following practical conventions but also simplifying for the sake of illustration, we store $\sigma(\cdot, \cdot)$ on a $|\mathcal{S}| \times |\mathcal{T}|$ grid, where \mathcal{S} contains $|\mathcal{S}|$ equally-spaced price points in

$[S_{\text{surface}}^{\min}, S_{\text{surface}}^{\max}]$ and \mathcal{T} contains $|\mathcal{T}|$ equally-spaced time points in $[t_{\text{surface}}^{\min}, t_{\text{surface}}^{\max}]$. At each point on the grid, we store the value of local volatility according to [Carmona \(2007\)](#):

$$\sigma_{\text{base}}^2(x, t) = \frac{\sum_{i=0}^2 p_i \tau_i e^{-x^2/(2t\tau_i^2) - t\tau_i^2/8}}{\sum_{i=0}^2 (p_i/\tau_i) e^{-x^2/(2t\tau_i^2) - t\tau_i^2/8}}, \quad \text{with } p_0 := 1 - p_1 - p_2, \quad x := \log(S_t/S_0), \quad (15)$$

for $p_0 = 0.3, p_1 = 0.5, p_2 = 0.2, \tau_0 = 0.4, \tau_1 = 0.3, \tau_2 = 0.6$ as in Figure 2 in [Carmona \(2007\)](#). While this analytical form (15) is used in our data-generating process, it is important to note that PEMC treats the surface as any market-calibrated volatility surface - accessing it only through its discrete grid values. When sampling $\theta \sim \Theta$ to produce σ grid, we add a $\mathcal{N}(0, \xi^2)$ noise independently to all the $|\mathcal{S}| \times |\mathcal{T}|$ points in the grid, on top of their baseline value σ_{base} (15). A path is then generated by Euler's scheme:

$$\begin{aligned} v_{t+\Delta t} &\leftarrow v_t + \kappa(\eta_t - v_t)\Delta t + \delta \Delta W_t^\nu, \\ S_{t+\Delta t} &\leftarrow S_t \exp\left(\left(r - \frac{1}{2}\tilde{v}_{t+\Delta t}^2\right)\Delta t + \tilde{v}_{t+\Delta t} \Delta W_t^S\right), \quad \text{where } \tilde{v}_{t+\Delta t} = \widehat{\sigma}(S_t, t) e^{v_{t+\Delta t}}, \end{aligned}$$

with $(\Delta W_t^S, \Delta W_t^\nu) \stackrel{\text{i.i.d.}}{\sim} \sqrt{\Delta t} \cdot \mathcal{N}(\mathbf{0}, \begin{bmatrix} 1 & \rho \\ \rho & 1 \end{bmatrix})$, and $\widehat{\sigma}(S_t, t)$ obtained by interpolations of the grid σ . The input (θ, X) can be represented as

$$\text{feature}_i = \underbrace{\{\{\sigma^{(s,t)}\}_{s \in \mathcal{S}, t \in \mathcal{T}}\}}_{\text{surface info}}, \underbrace{r, \delta, \kappa, \rho, \mu}_{\theta_{\text{model}}}, \underbrace{S_0, v_0}_{\theta_{\text{simulation}}}, \underbrace{K}_{\theta_{\text{payoff}}}, \underbrace{(W_T^S, W_T^\nu)}_{\mathbf{X}(\theta)}\}.$$

The parameters space Θ , as well as the evaluation θ , is summarized in Table 6.

Table 6 Parameter Setup in SLV Model

mode	ξ	S_0	r	κ	λ	ρ	$T, \Delta t$
$N_{\text{train}} = 3,000,000$	0.02	[50, 150]	0.02	[1.5, 4.5]	[0.1, 1.0]	[-0.2, -0.9]	1, 1/252
evaluation	0	100	0.02	3.0	0.5	-0.5	

To handle the 2D grid of high-dimensional volatility surface data, we design a two-branch neural network architecture, which is illustrated in Figure 4. The first branch processes the discretized volatility surface $\sigma^2(x, t)$ using a CNN architecture inspired by VGG ([Simonyan](#)

and Zisserman 2014), which has become a standard choice for image processing tasks and is readily available in modern deep learning packages like PyTorch (Paszke et al. 2019). This branch then consists of two 2D convolutional layers interspersed with ReLU activations, followed by a MaxPool2d operation for dimensionality reduction. The surface features are then flattened through a fully connected layer to produce an embedding. The second branch handles the remaining model parameters in (θ, X) through a series of fully connected layers with dropout regularization, batch normalization, and ReLU activations, ultimately producing another embedding. Finally, the two separate embeddings are then fed into a ‘‘Synthesizer’’ module, which combines the information through additional fully connected layers with dropout and ReLU activations to produce the final prediction. This architecture choice is motivated by the proven effectiveness of CNNs in handling grid-structured data (LeCun et al. 1998, He et al. 2016), and particularly the VGG architecture’s success in extracting hierarchical features while maintaining relative simplicity (Simonyan and Zisserman 2014). The details of NN architecture are summarized in Table 7.

Table 7 Neural Network Architecture Parameters

CNN Branch	Feed-forward Branch
kernel size: 3, stride: 1, padding: 1	hidden dim: 512
max pooling (kernel: 2, stride: 2, padding: 0)	output dim: 128

Using the same experimental setup as before, we evaluate PEMC’s performance in the SLV setting across sample sizes $n \in \{1000, 2000, 4000, 8000, 10000, 20000\}$ with $N = 10n$, benchmarking against a ground truth computed from 5×10^7 MC samples. The results, based on 200 independent experiments and shown in Table 8, reveal that PEMC’s effectiveness persists even in this more complex setting. Despite the added complexity of handling high-dimensional volatility surfaces, PEMC achieves a 30-40% reduction in mean squared error compared to standard MC, demonstrating its robustness as a variance reduction technique across different model frameworks.

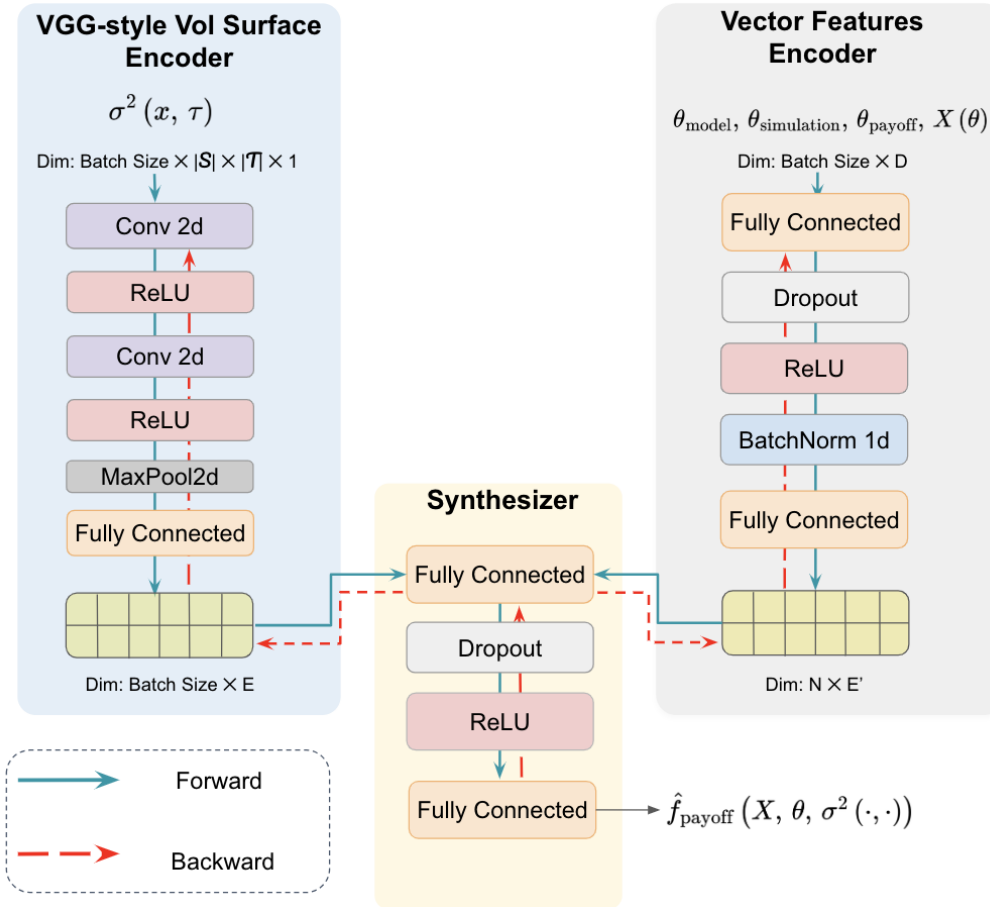


Figure 4 Neural Network architecture for the SLV Model.

Table 8 RMSE from 200 Experiments for Pricing Variance Swap under the SLV Model

Method	$n = 1000$	$n = 2000$	$n = 4000$	$n = 6000$	$n = 8000$	$n = 10000$	$n = 20000$
Monte Carlo (MC)	0.0206	0.0145	0.0101	0.0075	0.0064	0.0065	0.0047
PEMC	0.0130	0.0088	0.0061	0.0055	0.0040	0.0040	0.0027

4.2. Swaptions in HJM Models

Interest rate derivatives play a crucial role in financial markets, with swaptions being particularly important instruments for managing interest rate risk (Brigo and Mercurio 2006). A swaption gives its holder the right to enter into an interest rate swap at a future date, providing flexibility in hedging future interest rate exposures (Hull 2018). The pric-

ing of these instruments, however, presents significant computational challenges due to the high-dimensional nature of interest rate modeling (Andersen and Piterbarg 2010). In this subsection, we demonstrate PEMC's application to swaption pricing under the Heath-Jarrow-Morton (HJM) framework (Heath et al. 1992). The HJM model directly describes the evolution of the entire forward rate curve, offering greater flexibility than traditional short-rate models. For illustration purposes, we focus on a one-factor specification with exponential volatility structure (Glasserman 2013b), though the framework readily extends to multi-factor cases. This model choice represents a balance between analytical tractability and practical relevance, allowing us to demonstrate PEMC's effectiveness in a high-dimensional setting while maintaining computational feasibility.

4.2.1. Swaptions and HJM Model A swaption is a contract granting its holder the right, but not the obligation, to enter into an interest rate swap at a future date. In a standard interest rate swap, one party agrees to pay a fixed rate while receiving a floating rate, and the other party does the opposite. Consider a swap with n_p fixed payment periods, each of length $\Delta t'$, starting at time t'_0 and ending at time $t'_{n_p} = t'_0 + \sum_{l=1}^{n_p} \Delta t'$. The value of this swap at time t'_0 is:

$$V_{t'_0} = C \left(R \sum_{l=1}^{n_p} B(t'_0, t'_l) \Delta t' + B(t'_0, t'_{n_p}) - 1 \right),$$

where C is the notional amount (contract size), R is the fixed rate, and $B(t'_0, t'_l)$ is the discount factor from t'_0 to t'_l . A swaption provides the holder with the option to enter into this swap at t'_0 . The payoff of the swaption is simply

$$\max(0, V_{t'_0}),$$

and its expectation under the risk-neutral measure gives the price of swaptions. To specify the risk neutral measure, one needs to model the bond price. The price of a zero-coupon bond $B(t, T)$ maturing at time T is given by the forward rate $f(t, u)$ as: $B(t, T) =$

$\exp\left(-\int_t^T f(t, u) du\right)$, or equivalently $\frac{\partial \log B(t, T)}{\partial T} = -f(t, T)$. The HJM framework (Glasserman 2013b) then models the dynamics of forward rate curve directly:

$$df(t, T) = \mu(t, T) dt + \sigma(t, T)^\top dW(t),$$

where $\mu(t, T)$ is the drift, $\sigma(t, T)$ is the volatility function of the forward rate, and $W(t)$ is a Brownian motion. In contrast to short-rate models (e.g., Vasicek (Vasicek 1977) or Cox-Ingersoll-Ross (Cox et al. 1985)), which only model the dynamics of the short-term interest rate, the HJM model directly models the dynamics of the entire term structure of interest rates (Heath et al. 1992). The HJM model is widely used in practice because of its flexibility in modeling interest rate derivatives like swaptions and its ability to incorporate complex volatility structures (Brigo and Mercurio 2006, Andersen and Piterbarg 2010). However, the model's generality also leads to the need for sophisticated numerical methods for simulation Glasserman (2013b). A key property of the HJM model is the no-arbitrage condition (Glasserman 2013b), which specifies the drift completely by the volatility:

$$\mu(t, T) = \sigma(t, T)^\top \int_t^T \sigma(t, u) du. \quad (16)$$

Thus, in the HJM framework, the model is fully specified by defining the initial forward rate curve $f(0, T)$ and the structure of the volatility $\sigma(t, T)$. In our experiment we used a simple one factor HJM for illustration.

4.2.2. PEMC for HJM Just as with the local volatility surface case, in practice $\sigma(t, T)$ cannot be predefined parametrically and must be calibrated from market data of caps, floors, and swaptions, yielding a discrete grid of values. However, for demonstration purposes, we employ a classical exponential decay specification as our baseline model inspired from Glasserman (2013b):

$$\sigma_{base}(t, T) = \sigma_0 \exp(-\alpha_\sigma(T - t)) \quad (17)$$

with σ_0 and α_σ as part of θ . Similarly, for a baseline initial forward curve, we use:

$$f_{base}(0, T) = f_0 + c_f(1 - \exp(-\alpha_f T)). \quad (18)$$

with f_0 , c_f , and α_f part of the θ . While this analytical form serves as our data-generating process, PEMC accesses it only through its discrete grid values with added noise. This approach mirrors our treatment of the local volatility surface in the previous section, where we used the parametric form in [Carmona \(2007\)](#) solely as a realistic baseline for generating training data.

Indeed, while HJM and these analytical forms (17)-(18) are formulated in continuous time, in practice we need to implement numerical discretization. Following the scheme in [Glasserman \(2013b\)](#), one discretizes both the time axis and the set of maturities i.e., time steps $\mathcal{T}_t = \{t_0, t_1, \dots, t_{N_T}\}$ and maturity points $\mathcal{T} = \{t_1, t_2, \dots, t_{N_M}\}$ forming a time-maturity grid. In our experiment, for simplicity, we assume they share one grid \mathcal{T} of size $|\mathcal{T}|$. Then, when sampling $\theta \sim \Theta$, one first sample $\sigma_0, \alpha_\sigma, f_0, c_f, \alpha_f$, then one sample the grids $\{\sigma(t_i, t_j)\}_{t_i \leq t_j, t_i, t_j \in \mathcal{T}}$ and $\{f(0, t_i)\}_{t_i \in \mathcal{T}}$ from (17) and (18) with added noise $\mathcal{N}(0, (\frac{\sigma_0}{2(t_j+5)})^2)$ and $\mathcal{N}(0, (\frac{1}{100(t_j+5)})^2)$ respectively, on top of their baseline values. The noise level $\xi = \frac{\sigma_0}{2(t+5)}$. Paths are then generated using the discretization scheme described in [Glasserman \(2013b\)](#) (e.g., $f(t_i, t_j) = f(t_{i-1}, t_j) + \mu(t_{i-1}, t_j)(t_i - t_{i-1}) + \sqrt{t_i - t_{i-1}}\sigma(t_{i-1}, t_j)\mathcal{N}(0, 1)$ where $\mu(t_{i-1}, t_j)$ is the discretized drift term determined through (16)). We refer interested readers to [Glasserman \(2013b\)](#) for the complete derivation and implementation details of this standard simulation scheme.

For PEMC, our the parameter $\theta \sim \Theta$ includes the volatility parameters $(\sigma_0, \alpha_\sigma)$ in (17) and initial forward curve parameters (f_0, c, α_f) in (18). The swaption's fixed rate is set as $R = \exp(-\frac{\sum_i^{n-1} f(0, t'_i)}{T_{\text{final}} - t'_0})$, reflecting the common practice where swap rates are typically determined in reference to the prevailing forward rate curve rather than being arbitrarily chosen. Here the parameters are notional amount C , start time t'_0 , payment interval $\Delta t'$, and number of payments n_p . The simulation uses time step Δt up to final maturity T_{final} . During training, parameters are sampled uniformly from the ranges specified in [Table 9](#) where the evaluation θ is also listed.

Table 9 Parameter Setup in HJM Model

Mode	σ_0	α_σ	f_0	c_f	α_f	R	C	t'_0	$\Delta t'$	n_p	Δt	T^*
$N_{\text{train}} = 3,000,000$	[0.01, 0.03]	[0.001, 0.9]	[0.01, 0.03]	[0.01, 0.05]	[0.001, 0.9]	$\exp(-\frac{\sum_{i=0}^{n-1} f(0, t'_i)}{T^* - t'_0})$	100	5	1	20	1/52	25
evaluation	0.0015	100	0.02	3.0	0.5							

The input for PEMC is, similar as before:

$$\text{feature} = \underbrace{\{\{\sigma(t_i, t_j)\}_{t_i \leq t_j, t_i, t_j \in \mathcal{T}}\}}_{\text{volatility structure}}, \underbrace{\{\sigma_0, \alpha_\sigma, f_0, c_f, \alpha_f\}}_{\theta_{\text{model}}}, \underbrace{\{f(0, t_i)\}_{t_i \in \mathcal{T}}}_{\text{initial forward curve}}, \underbrace{(W_T^S, W_T^V)}_{\mathbf{X}}.$$

To handle both the two-dimensional grid of volatility structure $\sigma(t, T)$ and the one dimensional grid of initial forward curve $f(0, T)$, we design a three-branch neural network architecture, illustrated in Figure 5. The first branch, labeled “2D Function Encoder”, processes the 2d volatility structure grid using a CNN architecture with two 2D convolutional layers, each followed by batch normalization. The branch concludes with an average pooling operation and produces an embedding. The second branch processes the initial forward curve $f(0, T)$ grid through a “1D Function Encoder” utilizing 1D convolutional layers - a natural choice for sequential data (LeCun et al. 1998) - followed by batch normalization and average pooling to produce another embedding. The third branch handles the remaining input through fully connected layers with batch normalization. Finally, these three separate embeddings are then fed into a “Synthesizer” module that combines the information through multiple fully connected layers with batch normalization, ultimately producing the final prediction. This architecture effectively leverages both the spatial structure of the volatility surface through 2D CNNs (Simonyan and Zisserman 2014), the sequential nature of the forward curve through 1D CNNs (Oord et al. 2016), and the scalar parameters through standard deep learning techniques (He et al. 2016). The complete network architecture is detailed in Table 10.

Finally, following the same evaluation methodology, we assess PEMC’s performance in the HJM swaption pricing setting across sample sizes $n \in \{1000, 3000, 5000, 7000, 9000, 11000\}$ with $N = 10n$, using 5×10^7 MC samples to establish the ground truth value. As presented in Table 11, the outcomes from 200 independent

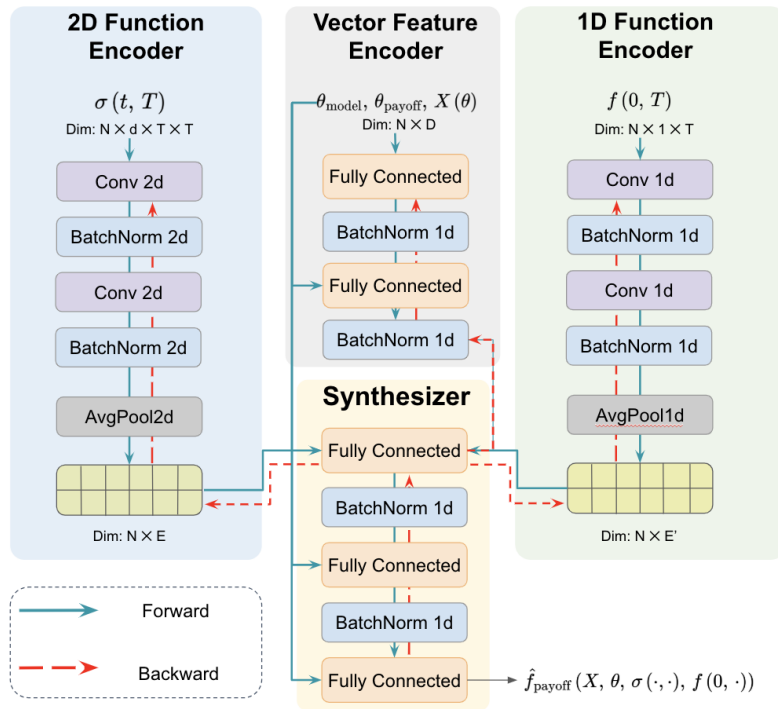


Figure 5 Neural network architecture for modeling Swaption payoff.

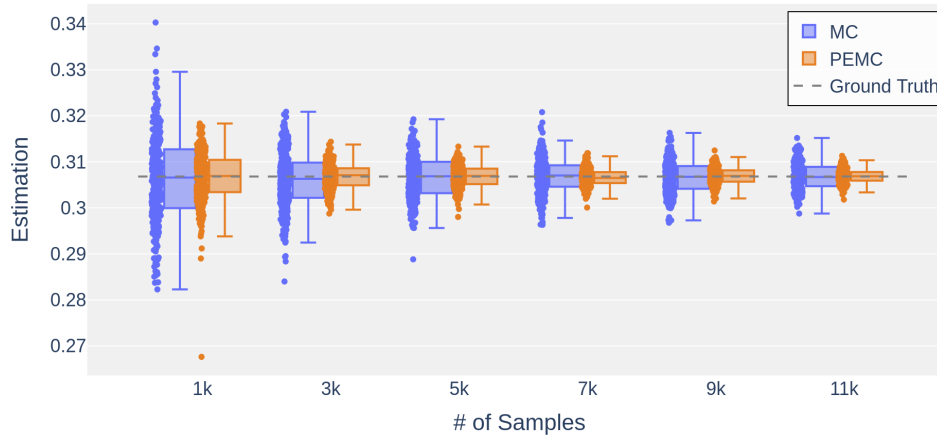
2D function branch parameters	1D function branch parameters	Vector feature branch parameters
Kernel size: (1, 3)	Kernel size: 10	
Stride: (1, 3)	Stride: 3	
Padding: 0	Padding: 0	Hidden dim: 512
AvgPool2d kernel size: (2, 2)	AvgPool1d kernel size: 2	Output dim: 128
AvgPool2d stride: (2, 2)	AvgPool1d stride: 2	
AvgPool2d padding: 0	AvgPool1d padding: 0	
Feed-forward Synthesizer Parameters		
Hidden dim: 128		
Output dim: 1		

Table 10 Hyper-parameter setup for the neural network

experiments confirm that PEMC remains highly effective within the context of interest rate derivatives. Despite the added complexity of managing both volatility structures and forward rate curves, PEMC achieves a 45-50% reduction in RMSE to standard Monte Carlo methods. This performance aligns with the variance reduction levels observed in our earlier examples. The boxplot is shown in Figure 4.2.2. The consistent effectiveness of PEMC across various financial instruments and modeling frameworks further underscores its versatility as a robust variance reduction technique.

Table 11 Root Mean Squared Error from 200 Experiments

Method	$n = 1000$	$n = 3000$	$n = 5000$	$n = 7000$	$n = 9000$	$n = 11000$
Monte Carlo (MC)	0.0096	0.0062	0.0048	0.0039	0.0035	0.0029
PEMC	0.0055	0.0028	0.0024	0.0019	0.0018	0.0015



Boxplots for HJM Experiments.

4.3. Discussions and Extensions

We conclude with several practical observations and potential extensions of the PEMC framework.

4.3.1. Evaluation Metric First, while training the neural network estimator g using mean squared error (MSE) loss is common, it is not always clear how to interpret the resulting MSE score. Unlike some well-established benchmarks (e.g., classification accuracy), there is no canonical threshold or known “good” MSE value for a given problem. This ambiguity makes it challenging to determine when the network is sufficiently trained. To address this, we can exploit the fact that g is meant to represent the conditional expectation $g = \mathbb{E}[f \mid \text{input}]$. If the network approximates this expectation well, then the sample average of $g(\mathbf{X})$ should be close to the sample average of $f(\mathbf{Y})$ over a given dataset. One practical diagnostic is to compute the Mean Absolute Relative Error (MARE) between these two averages. If $\mathbb{E}[g(\mathbf{X})] \approx \mathbb{E}[f(\mathbf{Y})]$, it provides a tangible indication that g is capturing the underlying expectation. Our empirical experience suggests this criterion is very effective in practice (a 5-1% MARE typically indicates exceptional PEMC), complementing common techniques like early stopping in machine learning workflows. More importantly, as we have shown in the theory, if g closely approximates the conditional expectation, the variance reduction in PEMC is guaranteed—even if marginally—relative to standard Monte Carlo.

4.3.2. XVA, Greeks and Quasi-Monte Carlo Beyond pricing exotic options, this approach naturally extends to other computationally intensive Monte Carlo settings in quantitative finance. Notably, adjustments like Credit valuation adjustment (CVA) and more complex XVAs often require vast simulation runs, sometimes taking days to complete (Green et al. 2015, Andersen et al. 2017). Integrating PEMC with a well-trained neural network can cut these computational times drastically while preserving accuracy.

Moreover, in the pricing of exotic derivatives and other path-dependent instruments, automatic differentiation (AD) techniques are often used to compute Greeks efficiently. By leveraging modern deep learning frameworks—such as PyTorch or TensorFlow—that support automatic differentiation natively, we can easily differentiate the trained network g with respect to input parameters (Giles and Glasserman 2006). This enables quick and accurate sensitivity analysis without resorting to finite-difference approximations or nested simulations, which could lead to another direction of extension for PEMC.

Finally, although we have focused on standard Monte Carlo sampling, combining PEMC with Quasi Monte Carlo (QMC) techniques may offer further variance reduction benefits (Caffisch 1998). However, it is important to note that QMC methods introduce a low-discrepancy bias, thus forgoing the unbiasedness property of pure Monte Carlo. Balancing unbiasedness with the additional variance reduction from QMC is an intriguing direction for future research.

5. Conclusion

In this paper, we introduced the Prediction-Enhanced Monte Carlo (PEMC) framework, a novel approach that leverages machine learning-based predictors to serve as flexible, data-driven control variates. By doing so, we preserve the unbiasedness of Monte Carlo estimators while significantly enhancing their efficiency in complex settings where traditional variance reduction techniques such as control variates are difficult or impossible to construct.

We demonstrated the practical value of PEMC through applications: pricing variance swaps under both a Heston and a Stochastic Local Volatility model, and pricing swaptions under the Heath-Jarrow-Morton framework. These examples, each introducing their own modeling and computational challenges, highlight PEMC's versatility and effectiveness.

While we have demonstrated the power of the PEMC framework on an options pricing application, we believe PEMC represents a new frontier for variance reduction, blending modern machine learning methodologies with classical Monte Carlo simulation.

A promising avenue for future research is to explore the connection between PEMC and meta-learning, which seeks to develop models capable of learning how to construct effective control variates from related problems. This approach reduces the need for problem-specific tuning, as demonstrated by Finn et al. (2017). Additionally, the recent surge in consistency models and diffusion-based generative techniques in machine learning (Ho et al. (2020), Song et al. (2021)) opens up new possibilities. While their direct application to pricing and control variates remains largely unexplored, these flexible generative models

could, in theory, produce advanced proposal distributions or control variates. Nonetheless, significant methodological and theoretical gaps must be bridged before such methods can be integrated seamlessly and rigorously into financial computation pipelines.

Another intriguing direction lies in leveraging recent advancements in causal inference and robust statistics, particularly methods designed to handle shifts in underlying data distributions (see Li and Lam (2020), Bodnar et al. (2022), Ellickson et al. (2023), Kang and Schafer (2007), Hernán and Robins (2020)). For instance, studies such as Angelopoulos et al. (2023), Li and Lam (2020), Quionero-Candela et al. (2009), Bickel et al. (2009), Sugiyama and Kawanabe (2009) propose robust regression techniques under covariate shift. These advances suggest that methodologies initially developed for causal inference—designed to ensure stability against model misspecification and distributional drift—could inform the creation of more versatile and robust variance reduction schemes. Incorporating ideas from doubly robust estimators into the ML-based control variate framework could pave the way for hybrid methods like PEMC to better handle uncertain or dynamic environments.

References

- Abadi M, Barham P, Chen J, Chen Z, Davis A, Dean J, Devin M, Ghemawat S, Irving G, Isard M, et al. (2016) Tensorflow: Large-scale machine learning on heterogeneous distributed systems. ArXiv preprint arXiv:1603.04467.
- Andersen L (2008) Simple and efficient simulation of the heston stochastic volatility model. *Journal of Computational Finance* 11(3):1–43.
- Andersen L, Duffie D, Song Y (2017) Xva challenges. *Quantitative Finance* 19(1):1–38.
- Andersen LB, Piterbarg VV (2010) Interest rate modeling. *Atlantic Financial Press* 1.
- Angelopoulos AN, Bates S, Fannjiang C, Jordan MI, Zrnic T (2023) Prediction-powered inference. *Science* 382(6671):669–674.
- Anthony M, Bartlett PL (1999) *Neural Network Learning: Theoretical Foundations* (Cambridge University Press).

- Arora S, Ge R, Ma T, Zhang Y (2018) Stronger generalization bounds for deep nets via a compression approach. *International Conference on Machine Learning (ICML)*, 254–263.
- Asmussen S, Glynn PW (2007) *Stochastic Simulation: Algorithms and Analysis* (New York: Springer).
- Bang H, Robins JM (2005) Doubly robust estimation in missing data and causal inference models. *Biometrics* 61(4):962–973.
- Bartlett PL, Foster DJ, Telgarsky M (2017) Spectrally-normalized margin bounds for neural networks. *Advances in Neural Information Processing Systems (NeurIPS)*, 6240–6249.
- Bartlett PL, Mendelson S (2002) Rademacher and gaussian complexities: Risk bounds and structural results. *Journal of Machine Learning Research* 3(Nov):463–482.
- Bartlett PL, Mendelson S (2005) Local rademacher complexities. *Annals of Statistics* 33(4):1497–1537.
- Bayer C, Derman E, Gourlay I, Scott M (1999) Variance swaps and options on variance. *Risk Magazine* 12(9):75–78.
- Bayer C, Stepper B (2019) Deep pricing: Financial derivative pricing with deep learning. *Journal of Mathematics in Industry* 9(1):1–15.
- Ben-Tal A, El Ghaoui L, Nemirovski A (2008) Robust optimization: methodology and applications. *Mathematical Programming* 114(1):1–33.
- Bickel S, Brückner M, Scheffer T (2009) Discriminative learning under covariate shift. *Journal of Machine Learning Research* 10:2137–2155.
- Bodnar LM, Cartus AR, Kennedy EH, Kirkpatrick SI, Parisi SM, Himes KP, Parker CB, Grobman WA, Simhan HN, Silver RM, et al. (2022) Use of a doubly robust machine-learning-based approach to evaluate body mass index as a modifier of the association between fruit and vegetable intake and preeclampsia. *American Journal of Epidemiology* 191(8):1396–1406, URL <http://dx.doi.org/10.1093/aje/kwac074>.
- Bottou L (2010) Large-scale machine learning with stochastic gradient descent. *Proceedings of COMP-STAT'2010*, 177–186 (Springer).
- Boyeau P, Angelopoulos AN, Yosef N, Malik J, Jordan MI (2024) Autoeval done right: Using synthetic data for model evaluation. *arXiv preprint arXiv:2403.07008* .
- Boyle P, Broadie M, Glasserman P (1997) Monte carlo methods for security pricing. *Journal of economic dynamics and control* 21(8-9):1267–1321.

- Bradbury J, Frostig R, Hawkins P, Johnson MJ, Leary C, Maclaurin D, Wanderman-Milne S, Zhang Q (2018) JAX: Composable transformations of Python+NumPy programs. <https://github.com/google/jax>.
- Brigo D, Mercurio F (2006) *Interest rate models-theory and practice: with smile, inflation and credit* (Springer Science & Business Media).
- Broadie M, Glasserman P (1996) Estimating security price derivatives using simulation. *Management Science* 42(2):269–285.
- Broadie M, Kaya Ö (2006) Exact simulation of stochastic volatility and other affine jump diffusion processes. *Operations research* 54(2):217–231.
- Buehler H, Gonon L, Teichmann J, Wood B (2019) Deep hedging. *Quantitative Finance* 19(8):1271–1291.
- Cafisch RE (1998) Monte carlo and quasi-monte carlo methods. *Acta numerica* 7:1–49.
- Carmona RA (2007) Hjm: A unified approach to dynamic models for fixed income, credit and equity markets. *Paris-Princeton Lectures on Mathematical Finance 2004* 1–50.
- Coleman TF, Li Y, Verma A (2001) Interpolation of implied volatility surfaces. *Computational Economics* 17:203–222.
- Cox JC, Ingersoll Jr JE, Ross SA (1985) A theory of the term structure of interest rates. *Econometrica* 385–407.
- Cybenko G (1989) Approximation by superpositions of a sigmoidal function. *Mathematics of Control, Signals and Systems* 2(4):303–314.
- Derman E, Fantazzini AE (1999) Pricing and hedging variance swaps. *Risk Magazine* 12(8):100–107.
- Derman E, Kani I (1994) Riding on a smile. *Risk* 7(2):32–39.
- Dingec KD, Sak H, Hörmann W (2015) Variance reduction for asian options under a general model framework. *Review of Finance* 19(2):907–949.
- Duffie D, Glynn P (1995) Efficient monte carlo simulation of security prices. *The Annals of Applied Probability* 5(4):897–905.
- Dupire B, et al. (1994) Pricing with a smile. *Risk* 7(1):18–20.
- Dziugaite GK, Roy DM (2017) Computing nonvacuous generalization bounds for deep (and shallow) learning with a pac-bayesian approach. *Uncertainty in Artificial Intelligence (UAI)*.

- Ellickson PB, Kar W, Reeder III JC (2023) Estimating marketing component effects: Double machine learning from targeted digital promotions. *Marketing Science* 42(4):704–728, URL <http://dx.doi.org/10.1287/mksc.2023.1427>.
- Esfahani PM, Kuhn D (2018) Data-driven distributionally robust optimization using the wasserstein metric: Performance guarantees and tractable reformulations. *Mathematical Programming* 171(1):115–166.
- Eyre B, Madras D (2024) Auto-evaluation with few labels through post-hoc regression. *arXiv preprint arXiv:2411.12665*.
- Ferguson M, Liang A (2018) Deep learning for pricing and hedging American-style options. *arXiv preprint arXiv:1812.11033*.
- Finn C, Abbeel P, Levine S (2017) Model-agnostic meta-learning for fast adaptation of deep networks. *International Conference on Machine Learning (ICML)*, 1126–1135.
- Fusai G, Meucci A (2008) Pricing discretely monitored asian options under lévy processes. *Journal of Banking & Finance* 32(10):2076–2088.
- Gatheral J (2006) *The Volatility Surface: A Practitioner's Guide* (John Wiley & Sons).
- Giles M, Glasserman P (2006) Smoking adjoints: Fast monte carlo greeks. *Risk* 19(1):88–92.
- Giles MB (2015) Multilevel monte carlo methods. *Acta Numerica* 24:259–328.
- Glasserman P (2013a) *Monte Carlo Methods in Financial Engineering*, volume 53 of *Stochastic Modelling and Applied Probability* (Springer).
- Glasserman P (2013b) *Monte Carlo methods in financial engineering* (Springer Science & Business Media).
- Green A, Kenyon C, Dennis C (2015) Xva: Credit, funding and capital valuation adjustments. *John Wiley & Sons*.
- Guyon J, Henry-Labordère P (2014) *Nonlinear Option Pricing* (Chapman and Hall/CRC).
- Hastie T, Tibshirani R, Friedman J (2009) *The Elements of Statistical Learning: Data Mining, Inference, and Prediction*, volume 2 (Springer).
- He K, Zhang X, Ren S, Sun J (2016) Deep residual learning for image recognition. *Proceedings of the IEEE Conference on Computer Vision and Pattern Recognition*, 770–778 (IEEE).
- Heath D, Jarrow R, Morton A (1992) Bond pricing and the term structure of interest rates: A new methodology for contingent claims valuation. *Econometrica* 77–105.

- Henderson SG, Glynn PW (2002) Optimization of control variate estimators. *Operations Research* 50(2):362–371, URL <http://dx.doi.org/10.1287/opre.50.2.362.424>.
- Henderson SG, Simon B (2004) Adaptive control variates for monte carlo simulation. *Naval Research Logistics* 51(4):348–364, URL <http://dx.doi.org/10.1002/nav.20011>.
- Hernán MA, Robins JM (2020) *Causal Inference: What If* (Boca Raton: Chapman & Hall/CRC).
- Heston SL (1993) A closed-form solution for options with stochastic volatility with applications to bond and currency options. *The review of financial studies* 6(2):327–343.
- Ho J, Jain A, Abbeel P (2020) Denoising diffusion probabilistic models. *Advances in Neural Information Processing Systems (NeurIPS)*, volume 33, 6840–6851.
- Hornik K (1991) Approximation capabilities of multilayer feedforward networks. *Neural Networks* 4(2):251–257.
- Horváth B, Muguruza A, Tomas M (2021) Deep learning volatility: a deep neural network perspective on pricing and calibration in (rough) volatility models. *Quantitative Finance* 21(1):11–27.
- Hull JC (2018) *Options, Futures, and Other Derivatives* (Boston: Pearson).
- Hutchinson JM, Lo AW, Poggio T (1994) A nonparametric approach to pricing and hedging derivative securities via learning networks. *The Journal of Finance* 49(3):851–889.
- Ioffe S, Szegedy C (2015) Batch normalization: Accelerating deep network training by reducing internal covariate shift. *International Conference on Machine Learning*, 448–456 (PMLR).
- Kang JDY, Schafer JL (2007) Demystifying double robustness: A comparison of alternative strategies for estimating a population mean from incomplete data. *Statistical Science* 22(4):523–539, URL <http://dx.doi.org/10.1214/07-STS227>.
- Karatzas I, Shreve SE (1991) *Brownian Motion and Stochastic Calculus*, volume 113 of *Graduate Texts in Mathematics* (Springer Science & Business Media), 2nd edition.
- Kim SH, Henderson SG (2007) Adaptive control variates for pricing multi-asset options. *Journal of Computational Finance* 10(2):57–82, URL <http://dx.doi.org/10.21314/JCF.2007.170>.
- Kingma DP, Ba J (2014) Adam: A method for stochastic optimization. *arXiv preprint arXiv:1412.6980*.
- Krizhevsky A, Sutskever I, Hinton GE (2012) Imagenet classification with deep convolutional neural networks. *Advances in Neural Information Processing Systems* 25:1097–1105.

- LeCun Y, Bottou L, Bengio Y, Haffner P (1998) Gradient-based learning applied to document recognition. *Proceedings of the IEEE* 86(11):2278–2324.
- Leluc G, Rossi M, Bolin D (2021) Learning control variates for monte carlo methods. *arXiv preprint arXiv:2112.01003* URL <https://arxiv.org/abs/2112.01003>.
- Leshno M, Lin VY, Pinkus A, Schocken S (1993) Multilayer feedforward networks with a nonpolynomial activation function can approximate any function. *Neural Networks* 6(6):861–867.
- Li F, Lam H (2020) Robust covariate shift regression. *Advances in Neural Information Processing Systems (NeurIPS)*.
- Li Z, Zhang Y (2023) Stein control variates for monte carlo. *Journal of Computational Physics* 476:111630, URL <http://dx.doi.org/10.1016/j.jcp.2023.111630>.
- Lord R, Koekkoek R, Dijk DV (2010) A comparison of biased simulation schemes for stochastic volatility models. *Quantitative Finance* 10(2):177–194.
- Lu Z, Pu H, Wang F, Hu Z, Wang L (2017) The expressive power of neural networks: A view from the approximation theory. *Advances in Neural Information Processing Systems (NeurIPS)*, 440–448.
- Maire S (2003) Monte carlo integration by l^2 -function approximation. *Journal of Computational and Applied Mathematics* 151:187–199, URL [http://dx.doi.org/10.1016/S0377-0427\(02\)00628-8](http://dx.doi.org/10.1016/S0377-0427(02)00628-8).
- Mohri M, Rostamizadeh A, Talwalkar A (2018) *Foundations of Machine Learning* (MIT Press), 2nd edition.
- Nair V, Hinton GE (2010) Rectified linear units improve restricted boltzmann machines. *Proceedings of the 27th International Conference on Machine Learning (ICML-10)* 807–814.
- Neyshabur B, Li Z, Bhojanapalli S, LeCun Y, Srebro N (2018) A pac-bayesian approach to spectrally-normalized margin bounds for neural networks. *International Conference on Learning Representations (ICLR)*.
- Oates CJ, Girolami M, Chopin N (2017) Control functionals for monte carlo integration. *Journal of the Royal Statistical Society: Series B (Statistical Methodology)* 79(3):695–718, URL <http://dx.doi.org/10.1111/rssb.12185>.
- Oord Avd, Dieleman S, Zen H, Simonyan K, Vinyals O, Graves A, Kalchbrenner N, Senior A, Kavukcuoglu K (2016) Wavenet: A generative model for raw audio. *arXiv preprint arXiv:1609.03499*.
- Paszke A, Gross S, Massa F, Lerer A, Bradbury J, Chanan G, Killeen T, Lin Z, Gimelshein N, Antiga L, et al. (2019) Pytorch: An imperative style, high-performance deep learning library. *Advances in Neural Information Processing Systems*, volume 32, 8024–8035 (Curran Associates, Inc.).

- Pinkus A (1999) Approximation theory of the mlp model in neural networks. *Acta Numerica* 8:143–195.
- Portier F, Segers J (2018) Monte carlo integration with a growing number of control variates. *Journal of Applied Probability* 55(4):1078–1092, URL <http://dx.doi.org/10.1017/jpr.2018.63>.
- Protter P (2010) *Variance and Volatility Swaps* (Hoboken, NJ: Wiley Finance).
- Quionero-Candela J, Sugiyama M, Schwaighofer A, Lawrence ND (2009) Dataset shift in machine learning. *Dataset Shift in Machine Learning* (Cambridge, MA: The MIT Press).
- Ren Y, Madan D, Qian MQ (2007) Calibrating and pricing with embedded local volatility models. *RISK-LONDON-RISK MAGAZINE LIMITED-* 20(9):138.
- Shen Z, Yang H, Zhang S (2021) Neural network approximation: Three perspectives. *Foundations of Computational Mathematics* 21(1):3–59.
- Simonyan K, Zisserman A (2014) Very deep convolutional networks for large-scale image recognition. *arXiv preprint arXiv:1409.1556* .
- Song Y, Sohl-Dickstein J, Kingma DP, Kumar A, Ermon S, Poole B (2021) Score-based generative modeling through stochastic differential equations. *International Conference on Learning Representations (ICLR)*.
- South L, Barthelmé S, Murray I (2022) Regularised control variates for variance reduction. *arXiv preprint arXiv:2202.12023* URL <https://arxiv.org/abs/2202.12023>.
- Srivastava N, Hinton G, Krizhevsky A, Sutskever I, Salakhutdinov RR (2014) Dropout: A simple way to prevent neural networks from overfitting. *Journal of Machine Learning Research* 15(1):1929–1958.
- Sugiyama M, Kawanabe M (2009) Covariate shift adaptation by importance weighted cross-validation. Quionero-Candela J, Sugiyama M, Schwaighofer A, Lawrence ND, eds., *Dataset Shift in Machine Learning*, 123–130 (Cambridge, MA: The MIT Press).
- Tataru G, Fisher T (2010) Stochastic local volatility. *Quantitative Development Group, Bloomberg Version* 1.
- Vapnik VN (1998) *Statistical Learning Theory* (Wiley).
- Vasicek O (1977) An equilibrium characterization of the term structure. *Journal of Financial Economics* 5(2):177–188.
- Vaswani A, Shazeer N, Parmar N, Uszkoreit J, Jones L, Gomez AN, Kaiser L, Polosukhin I (2017) Attention is all you need. *Advances in Neural Information Processing Systems*, volume 30, 5998–6008 (Curran Associates, Inc.).

- Yarotsky D (2017) Error bounds for approximations with deep relu networks. *Neural Networks* 94:103–114.
- Zrnic T, Candès EJ (2024) Cross-prediction-powered inference. *Proceedings of the National Academy of Sciences* 121(15):e2322083121.

Appendix

In this appendix, we go through the pipeline for a result in the form of Lemma 6 in Section 3.3.1. We begin by formally introducing the key concepts associated with the learning framework under consideration.

DEFINITION 2. Let g_0 denote the true regression function, defined by

$$g_0(\boldsymbol{\theta}, \mathbf{X}(\boldsymbol{\theta})) := \mathbb{E}_{\text{risk neutral measure}(\boldsymbol{\theta})} \left[f_{\theta_{\text{payoff}}}(\mathbf{Y}(\boldsymbol{\theta})) \mid (\boldsymbol{\theta}, \mathbf{X}(\boldsymbol{\theta})) \right]$$

$$= \arg \min_{g \text{ measurable}} \mathbb{E}_{\boldsymbol{\theta} \sim \Theta, (\mathbf{X}(\boldsymbol{\theta}), \mathbf{Y}(\boldsymbol{\theta})) \sim \text{risk neutral measure}(\boldsymbol{\theta})} \left(f_{\theta_{\text{payoff}}}(\mathbf{Y}(\boldsymbol{\theta})) - g(\boldsymbol{\theta}, \mathbf{X}(\boldsymbol{\theta})) \right)^2.$$

Note that equality exploits the well-known property of the squared loss minimizer: it is the conditional expectation of the target variable given the input features. The notable part is that, this formulation inherently incorporates the sampling over $\boldsymbol{\theta} \sim \Theta$. This is because, in PEMC we generate training data by first drawing $\boldsymbol{\theta}$ from Θ and then sampling $\mathbf{X}(\boldsymbol{\theta}), \mathbf{Y}(\boldsymbol{\theta})$ from the corresponding risk-neutral measure indexed by $\boldsymbol{\theta}$. However, since the result holds pointwise for each fixed $\boldsymbol{\theta} \in \Theta$, it also holds in the aggregate setting where $\boldsymbol{\theta}$ is (uniformly) random. For simplicity, we do not delve into technical measurability considerations here.

Next, we introduce the hypothesis class and define the best-in-class predictor. The hypothesis class \mathcal{G} plays a pivotal role in the learning framework, encapsulating the set of candidate functions from which the predictor g is selected.

DEFINITION 3. Let \mathcal{G} be the hypothesis class induced by the NN model family. Define g^* as the best-in-class function satisfying

$$g^*(\boldsymbol{\theta}, \mathbf{X}(\boldsymbol{\theta})) := \arg \min_{g \in \mathcal{G}} \mathbb{E}_{\boldsymbol{\theta} \sim \Theta, (\mathbf{X}(\boldsymbol{\theta}), \mathbf{Y}(\boldsymbol{\theta})) \sim \text{risk neutral measure}(\boldsymbol{\theta})} \left(f_{\theta_{\text{payoff}}}(\mathbf{Y}(\boldsymbol{\theta})) - g(\boldsymbol{\theta}, \mathbf{X}(\boldsymbol{\theta})) \right)^2$$

$$= \arg \min_{g \in \mathcal{G}} \mathbb{E}_{\boldsymbol{\theta} \sim \Theta, \mathbf{X}(\boldsymbol{\theta}) \sim \text{risk neutral measure}(\boldsymbol{\theta})} \left((g_0 - g)(\boldsymbol{\theta}, \mathbf{X}(\boldsymbol{\theta})) \right)^2.$$

where the second line follows again from the definition of g_0 . Considering a model g trained with N_{train} samples and is held fixed during the evaluation of the expectation, as is standard when discussing generalization error, the approximation error is defined as

$$\epsilon_a^{\mathcal{G}} := \mathbb{E}_{\boldsymbol{\theta} \sim \Theta, \mathbf{X}(\boldsymbol{\theta}) \sim \text{risk neutral measure}(\boldsymbol{\theta})} \left((g_0 - g^*)(\boldsymbol{\theta}, \mathbf{X}(\boldsymbol{\theta})) \right)^2,$$

and the statistical error from g obtained from training on N_{train} samples:

$$\epsilon_e^{N_{\text{train}}} := \mathbb{E}_{\theta \sim \Theta, \mathbf{X}(\theta) \sim \text{risk neutral measure}(\theta)} \left((g^* - g)(\theta, \mathbf{X}(\theta)) \right)^2.$$

Finally, define the total error as

$$\epsilon_{\text{total}} := \mathbb{E}_{\theta \sim \Theta, \mathbf{X}(\theta) \sim \text{risk neutral measure}(\theta)} \left((g_0 - g)(\theta, \mathbf{X}(\theta)) \right)^2.$$

It follows that

$$\epsilon_{\text{total}} \leq 2\epsilon_a^{\mathcal{G}} + 2\epsilon_e^{N_{\text{train}}}. \quad (19)$$

The interaction between $\epsilon_a^{\mathcal{G}}$ and $\epsilon_e^{N_{\text{train}}}$ essentially captures the bias-variance tradeoff. By choosing more expressive model classes (e.g., richer neural network architectures) and increasing the training set size, we can jointly reduce $\epsilon_a^{\mathcal{G}}$ and $\epsilon_e^{N_{\text{train}}}$. Thus, under reasonable conditions, ϵ_{total} can be made arbitrarily small if both $\epsilon_a^{\mathcal{G}}$ and $\epsilon_e^{N_{\text{train}}}$. In the following sections, we analyze $\epsilon_a^{\mathcal{G}}$ and $\epsilon_e^{N_{\text{train}}}$ respectively.

A. Approximation Error $\epsilon_a^{\mathcal{G}}$

Note that this best-in-class function g^* depends on the distribution of $\theta \sim \Theta$, meaning the notion of optimality is distribution-dependent on θ . This is also why we choose a distribution $\theta \sim \Theta$ that sufficiently covers the space. In this paper, \mathcal{G} is induced by our choice of neural network architecture and training procedure. The complexity of \mathcal{G} significantly impacts both approximation and statistical errors. Neural networks are renowned for their flexibility and expressiveness, serving as universal approximators. According to the Universal Approximation Theorem (Cybenko 1989, Hornik 1991), neural networks with a single hidden layer containing a sufficient number of neurons can approximate any continuous function on compact subsets of \mathbb{R}^n to arbitrary accuracy. Modern extensions of this theorem provide more nuanced insights into how network depth and architecture influence approximation capabilities (Yarotsky 2017, Lu et al. 2017, Shen et al. 2021, Cybenko 1989, Hornik 1991). Typical universal approximation theorems deals with compact input space in \mathbb{R}^n and point-wise convergence, in our context, we do not restrict \mathbf{X} to live in a compact space and we only need \mathcal{L}^2 convergence, so the theorem from Pinkus (1999) or Leshno et al. (1993) is sufficient, which gives us

LEMMA 7. *Suppose $g_0 : \Theta \times \mathbb{R}^{\dim(\mathbf{X})} \rightarrow \mathbb{R}$ is in $\mathcal{L}^2(\mathbb{P})$ where \mathbb{P} is the probability measure that governs the joint distribution of $\theta \sim \Theta$, $(\mathbf{X}(\theta), \mathbf{Y}(\theta)) \sim \text{risk neutral measure}(\theta)$. Then, for any $\epsilon > 0$, we can find a class of NN \mathcal{G} such that*

$$\epsilon_a^{\mathcal{G}} \leq \epsilon.$$

Proof See Pinkus (1999) or Leshno et al. (1993). \square

B. Statistical Error $\epsilon_e^{N_{\text{train}}}$

To quantify the capacity of \mathcal{G} , one could employ common complexity measures such as the Vapnik-Chervonenkis (VC) dimension (Vapnik 1998) or Rademacher complexity (Bartlett and Mendelson 2002). These measures provide bounds on the generalization error by capturing the richness of the hypothesis class. Modern studies have further refined our understanding of neural network complexity. For instance, norm-based capacity controls (Bartlett et al. 2017), PAC-Bayesian bounds (Dziugaite and Roy 2017), and local Rademacher complexities (Bartlett and Mendelson 2005) offer more nuanced insights. In particular, most neural network architectures are known to have finite complexity measures, such as finite VC dimension or other capacity metrics, when considered as a hypothesis class with a fixed number of parameters (Anthony and Bartlett 1999).

Consequently, when empirical risk minimization (ERM) is performed over these networks with controlled complexity, standard statistical learning theory guarantees apply, yielding generalization bounds that typically decrease on the order of $O(1/\sqrt{N_{\text{train}}})$ where N_{train} is the sample size (Bartlett et al. 2017, Neyshabur et al. 2018, Arora et al. 2018) and the constant in the rate depends on the complexity measure. Our PEMC prediction model can be considered as a ERM estimator. Thus, these results ensure that, given sufficiently large training sets and appropriate capacity constraints (e.g., weight regularization or architectural choices), neural networks can achieve low statistical error $\epsilon_e^{N_{\text{train}}}$.

Finally, there is an optimization error arising from the discrepancy between the empirical risk minimizer within \mathcal{G} and the final trained model g . This error accounts for situations where the optimization algorithm does not perfectly identify the empirical risk minimizer. However, we do not consider this optimization error, effectively assuming the presence of an ideal ‘‘oracle’’ for optimization. Consequently, theoretical analyses typically treat our g as readily available empirical minimizer.

LEMMA 8. *Suppose g is the empirical risk minimizer of Algorithm 1 and the neural network class \mathcal{G} has a finite VC-dimension or Rademacher complexity. Then, for any $\epsilon > 0$, there exists N_{train} such that*

$$\epsilon_e^{N_{\text{train}}} \leq \epsilon.$$

C. Proof of Lemma 6

Lemma 7 and Lemma 8 allows us to control ϵ_{total} using (19), which allows us to prove Lemma 6 with the help of the following technical definition and lemma.

DEFINITION 4. Define $\epsilon_{\text{total}}(\theta) := \mathbb{E}_{\mathbf{X}(\theta) \sim \text{risk neutral measure}(\theta)} (g(\mathbf{X}(\theta)) - g_0(\mathbf{X}(\theta)))^2$.

As a result, we have $\mathbb{E}_{\theta \sim \Theta} \epsilon_{\text{total}}(\theta) = \epsilon_{\text{total}}$, which allows us to establish the following lemma.

LEMMA 9. Let G be a second moment bound for g , i.e.,

$$\mathbb{E}_{\mathbf{X}(\boldsymbol{\theta}) \sim \text{risk neutral measure}(\boldsymbol{\theta})} g^2(\mathbf{X}(\boldsymbol{\theta})) \leq G.$$

uniformly for all $\boldsymbol{\theta} \in \Theta$. Then, for each $\boldsymbol{\theta} \in \Theta$,

$$|\sigma_f^2 - \sigma_g^2 - \sigma_{f-g}^2| \leq 2\sqrt{\epsilon_{\text{total}}(\boldsymbol{\theta})}\sqrt{G}.$$

Proof Fix any $\boldsymbol{\theta} \in \Theta$. From the variance decomposition, we have

$$\text{Var}(f) = \text{Var}(g) + \text{Var}(f - g) + 2 \text{Cov}(f - g, g),$$

which implies

$$|\sigma_f^2 - \sigma_g^2 - \sigma_{f-g}^2| \leq 2|\text{Cov}(f - g, g)|.$$

Conditioning on X and utilizing the properties of g_0 , we find that $\text{Cov}(f - g, g) = \text{Cov}(g_0 - g, g)$. Applying the Cauchy–Schwarz inequality yields the desired inequality. \square

We can now prove Lemma 6.

Proof of Lemma 6 Besides the assumptions in Lemma 7, Lemma 8 and Lemma 9, we further assume

$$g \leq \mathbb{E}_{\mathbf{X}(\boldsymbol{\theta}) \sim \text{risk neutral measure}(\boldsymbol{\theta})} g^2(\mathbf{X}(\boldsymbol{\theta})), \mathbb{E}_{\mathbf{Y}(\boldsymbol{\theta}) \sim \text{risk neutral measure}(\boldsymbol{\theta})} f^2(\mathbf{Y}(\boldsymbol{\theta})) \leq G, \quad (20)$$

for some $0 < g < G < \infty$, uniformly for all $\boldsymbol{\theta} \in \Theta$. Then, based on Lemma 7, 8 and Markov inequality, we can find \mathcal{G} and N_{train} such that, with probability at least $1 - \delta$, the randomly sampled $\boldsymbol{\theta} \sim \Theta$ satisfies

$$\epsilon_{\text{total}}(\boldsymbol{\theta}) \leq \epsilon,$$

which, together with Lemma 9 gives

$$|\sigma_f^2 - \sigma_g^2 - \sigma_{f-g}^2| \leq O(\epsilon),$$

with the constant in O not dependent on $\boldsymbol{\theta}$. Then, for at least $1 - \delta$ fraction of $\boldsymbol{\theta} \in \Theta$, as one shrinks $\epsilon \rightarrow 0$, $\epsilon_{\text{total}}(\boldsymbol{\theta}) \leq \epsilon$ and $|\sigma_f^2 - \sigma_g^2 - \sigma_{f-g}^2| \leq O(\epsilon)$ implies $\sigma_g^2 \rightarrow \sigma_{g_0}^2$ and $\sigma_{f-g}^2 \rightarrow \sigma_{f-g}^2$ uniformly for all such $\boldsymbol{\theta}$. Since $\sigma_f^2 = \sigma_{g_0}^2 + \sigma_{f-g}^2$, this further implies $\frac{\sigma_g}{\sigma_f} \rightarrow \frac{\sigma_{g_0}}{\sigma_f}$ and $\frac{\sigma_{f-g}}{\sigma_f} \rightarrow \frac{\sigma_{f-g_0}}{\sigma_f}$, given the boundedness of (20). Thus, $\frac{\text{Var}(PEMC)}{\text{Var}(MC)}$ in (7) $\rightarrow r(\rho, c)$ in (8), or equivalently, with probability at least $1 - \delta$, the randomly sampled $\boldsymbol{\theta} \sim \Theta$ satisfies

$$\frac{\text{Var}(PEMC)}{\text{Var}(MC)} = r(\rho, c) + O(\epsilon),$$

where the constant in O does not depend on $\boldsymbol{\theta}$. This concludes the proof. \square